Establishing a clinically relevant orthotopic xenograft model of patient-derived glioblastoma in zebrafish

Xiaolin Ai[1,2], Zengpanpan Ye[1,3], Chaoxin Xiao[1], Jian Zhong[1],

Joseph J. Lancman[4], Xuelan Chen[1], Xiangyu Pan[1], Yu Yang[1], Lin Zhou[1],

Xiang Wang[3], Huashan Shi[1], Dongmei Zhang[5], Yuqin Yao[6], Dan Cao[1*],

Chengjian Zhao[1*]

[1]State Key Laboratory of Biotherapy and Cancer Center, West China Hospital, Sichuan University, and Collaborative Innovation Center for Biotherapy, Chengdu 610041, Sichuan, P. R. China

[2]Department of Critical Care Medicine, West China Hospital, Sichuan University, Chengdu 610041, Sichuan, P. R. China

[3]Department of Neurosurgery, West China Hospital, Sichuan University, Chengdu 610041, Sichuan, P. R. China

[4]Human Genetics Program, Sanford Burnham Prebys Medical Discovery Institute, 10901 North Torrey Pines Road, La Jolla, CA 92037, USA

[5]Department of Gynecology and Obstetrics, West China Second University Hospital, Sichuan University, Chengdu 610041, Sichuan, P. R. China

[6]West China School of Public Health, No.4 West China Teaching Hospital, Sichuan University, Chengdu 610041, Sichuan, P. R. China

[*]Correspondence: caodan@wchscu.cn AND chjianzhao@scu.edu.cn (0000-0003-0624- 5263).

Summary statement

Zebrafish orthotropic GBM xenograft models contribute to clarify the genetic and biological study of GBM, identification of BBB-penetrating drugs and clinical sensitivity prediction of TMZ in GBM patients.

Additional information:

Correspondence author: Dan Cao, E-mail: caodan@wschscu.cn., Tel: 8615002880430, fax: 028-85582944; Chengjian Zhao, E-mail: chjianzhao@scu.edu.cn, Address:

Renmin Road No. 17, Chengdu 610041, Sichuan, P. R. China, Tel: 86-028-85164063, fax: 86-028-85164060.

Abbreviations:

Blood-brain-barrier (BBB); common cardinal vein (CCV); Dexamethasone (DEX); dpi (days post injection); epithelial-to-mesenchymal transition (EMT); endothelial cells (ECs); Glioblastoma (GBM); Gene Ontology (GO); Gene Set Enrichment analysis (GSEA); Magnetic Resonance Imaging (MRI); mouse PDOX models (mPDOX); optic tectum (TeO); Principal component analysis (PCA); patient-derived orthotopic xenograft models (PDOX); single cell RNA-seq (scRNA-seq); temozolomide (TMZ); zebrafish PDOX (zPDOX).

Abstract

An accurate prediction of the intracranial infiltration tendency and drug response of individual Glioblastoma (GBM) cells is essential for personalized prognosis and treatment for this disease. However, the clinical utility of mouse PDOX models remains limited given current technical constraints including difficulty in generating sufficient sample numbers from small tissue samples and a long latency period for results. To overcome these issues, we establish zebrafish GBM xenografts of diverse

origin, which can tolerate intracranial engraftment and maintain their unique histological features. Subsequent single cell RNA-seq (scRNA-seq) analysis confirms significant transcriptional identity resemble invading GBM microtumors observed in the proportionally larger brains of model animals and humans. Endothelial scRNA-seq confirms zebrafish blood-brain-barrier is homologous to the mammalian. Finally, we establish a rapid and efficient zebrafish PDOX (zPDOX) model, which can predict long-term outcomes of GBM patients within 20 days. zPDOX provides a novel avenue for precision medicine of GBM, especially for the evaluation of intracranial infiltration tendency and prediction of individual drug sensitivity.

Introduction

Glioblastoma (GBM) is the most common and lethal primary brain tumor. Despite considerable effort over the past 30 years dedicated to drug development in oncology, more than 90% of novel therapeutics fail in human trials(Hutchinson and Kirk, 2011; Zhou et al., 2020). There are numerous reasons for this high failure rate, the most significant of them being the lack of reliable preclinical models to screen therapeutics prior to use in patients(Kamb, 2005). In fact, many promising drug candidates for GBM have failed during the pre-clinical phases of development due to the blood–brain barrier (BBB)(Pardridge, 2005). In addition, developing efficient and reliable GBM animal models could enhance the drug discovery process for this disease and would be an especially powerful tool to stratify patient response for personalized medicine. To

address this need, patient-derived orthotopic xenograft models (PDOX) have been successfully established in mice, which allows the study of GBM pathogenesis and drug efficacy in the context of a whole animal(Kitange et al., 2009). However, the mouse-based GBM PDOX models are not widely used to evaluate tumor heterogeneity, for "co-clinical trials" or for rapid therapeutic screens. This is because their success rate is highly variable (0%~90%) and there is a long latency window following engraftment (2–11 months)(Patrizii et al., 2018; Xu et al., 2018). Therefore, to increase their utility, GBM PDOX models need to produce clinically relevant data faster.

One approach to improve GBM PDOX models is by establishing an alternative or complementary vertebrate model. Zebrafish larvae are one possibility and have advantages that can augment findings from rodent-based GBM PDOX model including immune tolerance, transparency for enhanced cellular resolution, and the speed at which large numbers of transplants can be performed(Ai et al., 2020; Shi et al., 2020; White et al., 2013). The use of zebrafish as a tumor xenograft model is supported by recent studies confirming that primary human tumors can robustly propagate in zebrafish larva (Fior et al., 2017; Mercatali et al., 2016). However, the zebrafish based GBM xenograft model is still not widely utilized in the brain tumor research field(Pudelko et al., 2018; Wehmas et al., 2016). There are several possible reasons for the lack of enthusiasm. First, in previous zebrafish studies, a thorough histopathological characterization of implanted GBM xenografts is lacking, leaving it unclear whether zebrafish GBM xenografts accurately phenocopy the specific

intracranial infiltration and vascularization features of the GBM observed in human and rodent models. Second, it is unclear whether zebrafish GBM xenograft can efficiently identify BBB-penetrating drugs with *in vivo* activity. Therefore, a profound understanding of pathological behaviors of implanted GBM cells and brain microenvironment of zebrafish larva, are fundamental to establishing the zebrafish model as a reliable human GBM orthotopic xenograft model and using it for therapeutic testing and drug screens.

Here, we begin the validation of the zebrafish GBM xenograft model by orthotopic injecting various GBM cells lines that differ in their infiltration and angiogenic properties. We demonstrate that all GBM tumor cells tested can robustly propagate in zebrafish brain and consistently recapitulate their unique pathological characteristics when growing in mammal brains. Next, by using BBB tracers and single-cell RNA-Seq, we demonstrate that the BBB in zebrafish larvae is functionally and molecularly homologous to the mammalian BBB. Basing on this information, by using primary patient derived GBM cells, we successfully established a reliable protocol for zebrafish based GBM PDOX and used it to evaluate the intracranial infiltration tendency and predict the long-term TMZ drug sensitivity of individual drug sensitivity. With these advances, we anticipate that the GBM zPDOX model can be widely adopted as a co-clinical test to rapidly define the unique intracranial infiltration potential and therapeutic response of individual patient's GBM sample. This new zPDOX model should shorten the time required to obtain the preclinical data needed for clinical

management of GBM and help further establish precision medicine for GBM as a viable clinical approach.

Materials and Methods

Transgenic Zebrafish Maintenance and Establishment. Lines used in this study included Tg(kdrl:EGFP)[s843], Tg(kdrl:mCherry)[uto2] and Nacre mutant (mitfaw2, skin-pigmentation mutation). To avoid pigmentation, we established kdrl:EGFP Nacre line by direct outcross and incross of kdrl:EGFP with Nacre fish. Zebrafish were maintained at 28.5°C with a 14-hour light and 10-hour dark cycle. Fish water was changed daily, and larva that more than 7 days old were fed twice a day with grinded brine shrimp. All zebrafish experiments were conducted in accordance with the guidelines of the Animal Care and Use Committee of Sichuan University (Chengdu, Sichuan, China) and approved by the institutional review board of the Medical Faculty at the West China Hospital, Sichuan University.

Glioma Cell Lines and Culture. Glioma cell lines, U87MG, U-251MG, GL261 and C6 were purchased from American Type Culture Collection (ATCC). These glioma cell lines were cultured in Dulbecco's modified Eagle's medium (DMEM) (Gibco), containing 10% fetal bovine serum (FBS) (Gibco) and 1:100 Pen/Strep (Invitrogen) at 37°C with 5% CO_2. Adherent cells were detached and dissociated with 0.025% trypsin

(Gibco) for 2 min. The GSCs (BNI-21, BNI-23) were cultured in Stem Cell Medium (neurobasal medium (Gibco) containing 2% B27 (Gibco), 10ng/ml bFGF (R&D Systems), 20ng/ml EGF (R&D Systems), Glutamax (Invitrogen), sodium pyruvate (Invitrogen) and antibiotics (Invitrogen)). All human cell lines used in this work were authenticated just prior to use. To establish stable mCherry-expressing glioma cell lines, wild-type glioma cells were infected with lentivirus containing a CMV driving mCherry gene. FACS (Aria, BD) was applied to sort the cells with same fluorescent intensity 48 hours post infection. The stable mCherry expressing cells were cultured in normal conditions.

Zebrafish Xenografts Injection. We tested to inject GBM cells into zebrafish brain at 2dpf, 3dpf, 4dpf and 5dpf, and compared the success rate and growth of implanted GBM xenograft respectively. We found that inject GBM cells at 3dpf can yield the higher success rate and allow a relative long observation window. The 5×10^6 mCherry-expressing glioma cells (U87MG, U-251MG, Gl261 and C6, ~100 cells per fish) were suspended in 50ul basic DMEM and loaded into a borosilicate glass needle pulled by a Flaming/Brown micropipette puller (Narishige, PN-30). Zebrafish larva at 3dpf (days post fertilization) were anesthetized with 0.2 mg/ml Tricaine (Sigma) before tumor injection. To establish the experimental zebrafish glioma model, 3~5 nanoliters suspension containing ~100 cells (Fig.S1) were injected into optic tectum (TeO) of kdrl:EGFP Nacre zebrafish larva (Fig.1B). Recipient zebrafish larva injected with

tumor cells were maintained in fish water containing the antibiotics at 33°C. After 24 hours post injection, zebrafish with cellular debris or cells in the ventricle were discarded. Around 100 tumor cells in midbrain parenchyma of zebrafish brain were regarded as successful injected zebrafish, and these injected zebrafish were randomly collected to each group separately until end of experiment.

Single-cell RNA seq for GBM cells implanted in zebrafish brain. We conducted single cell RNA seq to reveal transcriptome changes of GBM cells after implanting in zebrafish brain. The experimental strategy is outlined in Fig.2A. For GBM cells, zebrafish were injected with GBM-U-251MG-mCherry cells, and allowed to form widespread, tumor invasion for 4 days. At 4dpi, the brains of the zebrafish larva were isolated using tweezers. Under the fluorescence stereomicroscope, the core area and tumor invasion area of the glioma xenografts from the zebrafish brain were divided into two dishes, and completely disaggregated using 1mg/ml papain and 1mg/ml DNase at 37°C for 30min. After digestion, a single-cell suspension was made by resuspending the cells in DMEM with 2% FBS. Simultaneously, GBM-U-251MG-mCherry cells maintained in culture were trypsinized and resuspended in DMEM with 2% FBS. The mCherry positive single cells from cell suspension was sucked up into a vial containing lysis buffer by a borosilicate glass needle under fluorescence micromanipulation system (TransferMan NK 2, eppendorf). Four tumor cells from *in vitro* culture system, 9 tumor cells from the tumor core area and 8 tumor cells from the tumor invasion area

were sucked up to prepare single cell RNA sequence library. The single cell RNA sequence library was prepared according to Smart-seq2 protocol(Picelli et al., 2013). Samples were sequenced using the HiSeq2500 with approximately 20 million reads per sample, using 150-bp paired-end reads. The RNA-seq reads were aligned to the reference genome (GRCh39/GRCz10) by STAR_2.6.0a. Transcript abundance was normalized and measured in fragments per kb of exon per million fragments mapped (FPKM). Differential genes expression was analyzed by DESeq2. Genes with FDR ≤ 0.05 were counted as differentially expressed genes.

Principle component analysis (PCA) and Gene ontology (GO) analysis. We performed a PCA analysis of the gene expression values (FPKM) for all samples. In the PCA diagram, the samples between the groups should be dispersed, and the samples in the group should be brought together. In order to reflect the difference in gene expression between samples, we used the hierarchical clustering to cluster the gene expression values and homogenize the lines of expression data. Genes or samples with similar expression patterns in the heat map will be clustered together, and the color in each square reflects the expression of the gene. In addition, we used the GO database, which contained biological process and cellular component. The GO function enrichment uses p<0.05 as the threshold for significant enrichment. All heatmaps analyses were generated using the software Gene-E.

Single-cell RNA seq for endothelial cells of zebrafish. To detect BBB related gene expressed by endothelial cells (ECs) in zebrafish brain and the body trunk, the kdrl:EGFP zebrafish (5dpf, n=5) were used to obtain endothelial cells. Under the stereomicroscope, the brains of the zebrafish larva were isolated using tweezers. The brain and body trunk of zebrafish larva were divided into two dishes, and completely disaggregated. Under the fluorescence stereomicroscope, a single GFP expressing endothelial cell from cell suspension was sucked up by a borosilicate glass needle. Nine cerebral ECs and 3 body ECs were sucked up to prepare single cell RNA sequence library. The single cell RNA sequence library and data analyses was prepared following above.

Gene set enrichment analysis. BBB gene set contains 20 tight junction–related genes, 25 CLDN genes, 407 solute carrier transporters genes, and 53 ATP-binding cassette transporters genes). The zebrafish gene symbols were mapped to their human orthologues using the DIOPT tool (http://www.flyrnai.org/cgi-bin/DRSC_ orthologs.pl). From the zebrafish RNA-seq data set, we created a BBB related gene list of either upregulated or downregulated genes in the zebrafish cerebral endothelial cells versus trunk endothelial cells, and these were input into GSEA as GCT files. In addition, we used heat map to show the BBB related gene expression patterns between cerebral and body endothelial cells.

Pericardium microinjection of dextran, DAPI and NaF. In order to *in vivo* monitor the permeability of cerebral and body vessels in zebrafish, NaF (MW: 376 Da; Sigma), DAPI (MW: 350 Da; Sigma) and dextran blue (MW: 10,000; Invitrogen) were dissolved in PBS to final concentrations of 2 mg/ml, 1 mg/ml and 5 mg/ml respectively. About 5-10nl of tracers were injected into each common cardinal vein (CCV) using glass capillary needles. Injected zebrafish were washed twice with fresh fish water and confocal live images were taken within 1-2 hours post the tracer injection.

Human Tissue Processing and primary culture. All samples used for zPDOX establishment were obtained from the patients who were diagnosed with GBM by enhanced Magnetic Resonance Imaging (MRI) and pathological diagnosis at West China Hospital (Table S3). Written informed consent was obtained from all patients. Our study was approved by the institutional review board and the ethics committee of Sichuan University. The fresh GBM tissues were digested into single cells by Accutase (Sigma) for 30min at 37°C, and further washed with cold PBS (3 times) with gentle vortexing. The single cell suspensions were collected and passed through a 70-μm strainer (Milipore). These human primary GBM cells were cultured in three kinds of cell culture methods respectively, including organoid culture, neurosphere culture and adherent culture(Hubert et al., 2016). For 3-D organoid culture, red blood cells were removed by brief hypotonic lysis, and GBM cells were counted for cell number and viability using trypan blue. Around 105 of cells were mixed with 20μl Matrigel

(Corning), which were dropped into 24-well plate. Following solidify (15 min, 37 °C), the gels were overlaid with 500µl of Stem Cell Medium (neurobasal medium (Gibco) containing 2% B27 (Gibco), 10ng/ml bFGF (R&D Systems), 20ng/ml EGF (R&D Systems), Glutamax (Invitrogen), sodium pyruvate (Invitrogen) and antibiotics (Invitrogen)). For neurosphere culture(Jacob et al., 2020), resuspend the human GBM cells in 10-20 ml neurobasal medium plus all additives and incubate at 37 °C overnight. The next day, lysis red blood cells and change the media (Stem Cell Medium). The GBM stem cells were cultured for 1 week to form neurosphere. For adherent culture, human GBM cells were cultured in (DMEM/F12) (Gibco), containing 2% B27 (Gibco), 10ng/ml bFGF (R&D Systems), 20ng/ml EGF (R&D Systems), 5% fetal bovine serum (FBS) (Gibco) and 1:100 Pen/Strep (Invitrogen).

Establishment of zebrafish patient-derived orthotopic xenografts (zPDOX). To compare three kinds of cell culture methods in establishment of zPDOX models, we tried to injected human primary GBM cells into zebrafish brain from three kinds of cell culture methods, including organoid culture, neurosphere culture and adherent culture. Before injection, the cultured human primary GBM cells were digested into single cell suspensions. These cells were labeled *in vitro* using the CFSE vibrant cell labeling solution (Life Technologies), at a final concentration of 1 mmol/L in 0.1% BSA in DMEM for 30 minutes at 37C in a 5% CO_2 atmosphere, as previously reported. The CFSE labeled GBM cells were injected into zebrafish brain as described above. The

comparison of human GBM engraftment zebrafish brain at 3dpi was identified by Zeiss

LSM 880 Confocal Microscope.

Zebrafish Xenograft Drug Administration. In order to find a convenient and quick

zebrafish administration method for glioma xenografts, fluorescent NaF tracer (10μM)

and DAPI (1μM) was directly added into fish water containing zebrafish at 5dpf. And

the zebrafish was incubated for 2 hours (Fig.4A). Fluorescent staining of zebrafish was

detected by Zeiss LSM 880 confocal microscope and was used to monitor delivery

route of small molecular chemicals into the brain. Six anti-cancer drugs, associated

with treatment of glioma, were chosen from Selleck Ant Cancer Compound Library.

These six anti-cancer drugs, including Temozolomide (500μM), Vincristine

(10nM-20nM), Doxorubicin (1μM-2μM), Dexamethasone (10μM), Rapamycin

(25μM), and Gemcitabine (20μM), were tested *in vivo* and *in vitro*. Concentration of

these drugs were determined by zebrafish maximum tolerated concentration and

effective tumor concentrations tested *in vitro*. Zebrafish xenografts with the same

tumor size were randomly distributed in the treatment group and control group on 2dpi

(days post injection). Drugs were added directly into fish water, and the drug was

changed daily for continuing 3 days. Control group added the corresponding

concentration of DMSO. After 3 days of treatment, the regression of tumor in zebrafish

xenografts was identified under the fluorescence stereomicroscope. Tumor size was

determined by quantifying 2D image area using Image J and multiplying by the average mCherry fluorescence intensity.

zPDOX Temozolomide Administration Details. After a week of culture, human primary GBM cells were infected with lentivirus containing a CMV driving mCherry gene. The stably expressed mCherry GBM cells were injected into zebrafish brain as described above. The standard chemotherapy drug for high-grade GBM, temozolomide (TMZ), was used to test whether a short-term response to TMZ treatment in zPDOX would anticipate a delay in relapse in the matching patients. TMZ is dosed and administered as described above.

Hematoxylin Eosin (H&E) staining. The zebrafish xenograft was fixed in 4% paraformaldehyde (PFA), embedded in paraffin and sectioned at zebrafish brain tumor for 3μm thickness. Sections were stained with Hematoxylin and Eosin for routine histopathological analysis.

EdU Labeling. For EdU labeling, we add the EdU (500 mM) into the zebrafish water at 2dpi. And fixed the sample after 12h followed by using the Click-iT EdU Kit (Invitrogen) to label the proliferation cells according to the manufacturer's instruction.

Immunofluorescence. The *vitro* cultured human primary GBM cells were fixed in 4% formaldehyde. Primary antibodies used: anti-human Nestin (rabbit, ab105389), anti-human GFAP (mouse, ab10062), in general 1:100. Secondary antibodies Alexa goat anti-mouse 488 (1:400) and Alexa goat anti-rabbit 594 (1:400), nuclei were counterstained with DAPI.

Live Zebrafish Imaging Strategy and Qualification. For the entire zebrafish images, the anesthetized embryos were mounted in 0.08% Methyl cellulose. Both fluorescent and bright-field images were taken by Zeiss SteREO Discovery V20 stereomicroscope (Carl Zeiss, Germany). The whole brain of zebrafish was imaged with a Zeiss LSM 880 Confocal Microscope with Airyscan (Carl Zeiss) under 20× lens with a total depth of 100μm. For whole brain Z-stack images, maximum projection images were created from 100 um stacks (10 microns per confocal slice) using ZEN blue software (Carl Zeiss). Tumor size was determined by quantifying 3D image area of mCherry fluorescence using Inaris (Fig.S6). For digital living image of tumor proliferation and

angiogenesis, zebrafish embryos were mounted in low melting point (LMP) agarose (1.5%, wt/vol) at the bottom of a 29mm glass bottom dish and covered with fish water at 28°C. The micrographs images were taken with Zeiss LSM 880 Confocal Microscope with Airyscan (Carl Zeiss) under 20× lens with a total depth of 200μm. To calculate the infiltration distance of tumor cells from core margins, the infiltration distance of tumor cells was measured by the ZEN blue software (Carl Zeiss) and the digital tumor images were 3D-reconstructed by the Imaris software (Biplane). For detection of the BBB function in zebrafish larvae, the maximum projection images were analyzed by Profile in Zen blue, which showed fluorescence intensity of vascular and Dextran respectively.

Clinical Human GBM data. All of patients in our study receive the standard concurrent chemoradiotherapy after operation. The clinical data and specific chemoradiotherapy regimen of each patient was listed in Table S3. The surgeon had resected the tumor during the operation, and no tumor residue was found by postoperative MRI. The recurrence of GBM was confirmed by enhanced Magnetic Resonance Imaging (MRI) at 6-7 months after operation. The enhanced MRI images were assessed by two radiologists independently and disagreements were resolved by discussion or the involvement of the third radiologist.

Statistical Analysis. In all experiments, zebrafish were randomly assigned to experimental groups. Prism software was used for statistical analysis. All datasets were challenged by a normality test. Datasets with a Normal distribution were analyzed by unpaired t test. A level of *P< 0.05 or **P< 0.01 was regarded as statistically significant.

Results

Zebrafish orthotopic xenografts recapitulate the histological features of specific GBM tumor.

As the adaptive immune response of zebrafish is not fully established until the end of first month, our previous study has demonstrated that the zebrafish larva as a versatile host for orthotopic xeno-implantation of human glioma cells (U87MG and U-251MG)(Zeng et al., 2017; Zhao et al., 2018). However, to be considered reliable (or faithful), an orthotopic GBM xenograft model should accurately display the functional heterogeneity that is known to exist both within a tumor and between tumors. To assess the ability of the zebrafish model to reveal GBM heterogeneity, we compared the outcomes of zebrafish xenografts with what has been previously reported in rodent models for three of the most frequently used GBM cell lines (rat C6, human U87MG and mouse GL261).

To comprehensively track the intracranial invasion and vascularization of GBM xenografts within the zebrafish brain, we employed transparent Nacre/kdrl:EGFP zebrafish to visualize all vasculature using florescent microscopy (Fig.1A). By testing implantation at different stages with different cell numbers and volumes, we found that injecting ~100 GBM tumor cells (Fig.S1) into the optic tectum (TeO) of zebrafish larvae at 3dpf (days post fertilization) is optimal for GBM orthotopic xenograft (Fig.1B), yielding a high success rate and enabling a long observation time-window (about 10days) for tumor progression before lethality became significant.

Two days post injection (dpi), C6 xenografts initiate intensive infiltration along the cerebral capillaries with some of the invading C6 cells extending pseudopodia and migrating into parenchyma (Fig.1A and Fig.S2). However, despite extensive infiltration during the first week, tumor neovascularization was never detected in the tumor core of C6 xenografts in zebrafish brain (n=0/236). This is similar to the behavior of C6 cells in the brain of syngeneic Wistar rats, where a diffuse infiltrative growth pattern along with rare neovascularization is observed(Farin et al., 2006; Grobben et al., 2002).

We next tested the human U87MG cell line, which displays a distinct histopathological characteristic from the C6 cells. When orthotopically implanted in immunocompromised mice, U87MG tumor cells propagate as a well-demarcated tumor mass and rarely infiltrate into brain parenchyma. However, like GBM in patients, U87MG tumors are highly vascularized, making it the most commonly used GBM cells

to study GBM angiogenesis and evaluate anti-angiogenic therapeutics(Jacobs et al., 2011). Using the same approach for evaluating C6 glioma cells, we tracked the progression of U87MG xenografts in zebrafish brains for 1 week following implantation. From 2dpi, like the observation in mouse brain, U87MG xenografts initiate intensive angiogenesis and form complex tumor vasculature within the xenografts (Fig.1D). However, during this period, the number of U87MG cells invading into the surrounding parenchyma was very limited (Fig.1F, 1G).

At last, we tested the mouse GL261 GBM cell line, which displays many of the same histopathological features of primary human GBM. When implanted into the mouse brain, GL261 tumor cells are extremely infiltrative and induce extensive tumor angiogenesis within the tumor. As expected, like observations in the brain of syngeneic mice, GL261 xenografts in zebrafish brain display infiltrative growth pattern along with hyper-vascularization in the xenograft core (Fig.1E). Interestingly, compared to C6 and U87MG cells, we found that GL261 cells had distinct intracranial infiltration characteristics depending on their location. At the very front margin of infiltration, GL261 tumor cells prefer to invade along the host cerebral vessels, while GL261 cells closest to the tumor mass preferentially invade as cell groups into the parenchyma (Fig. 1F, 1G). These results indicate a highly heterogeneity of infiltrating patterns of GBM cells between tumors (Fig.1H).

Importantly, besides the distinct pathological features that displays by zebrafish orthotopic xenografts from the different GBM cell lines, we found that the pathological

phenotype within the intracranial xenografts from individual GBM cell line is extremely stable and homogenous (Fig.S3). As the GBM cell lines are genetically stable and has lost their intra-tumoral heterogeneity after passage cultivation(da Hora et al., 2019), thus we conclude that the zebrafish orthotopic xenografts faithfully reveals the intra-tumor heterogeneity between the tested GBM cell lines and the intra-tumor homogeneity within each tested GBM cell line.

In order to test patient derived GSCs in our zebrafish models, two GSCs (BNI-21, BNI-23)(Zhai et al., 2020) from Beijing Neurosurgical Institute GSCs bank that originally derived from primary GBM patients have been tested. These two GSCs have been implanted into the zebrafish brain as described previously. EdU staining of GCSs xenografts at 5dpi, showed the intensive GSCs proliferation in zebrafish brain (Fig.S4). Compared with GBM-BNI21, GBM-BNI23 showed a typical infiltrative growth pattern in zebrafish brain, indicating its potential usage in intracranial invasion studies. However, the growth pattern of both tested GCS cell lines within the zebrafish brain are stable and homogenous, which is similar to the previously tested serum grown glioma cell lines.

In summary, all tested GBM cells show their unique infiltrative and angiogenic pathological features when progressing in zebrafish brain (Fig.1H), matching what have been previously observed in rodent orthotopic models, demonstrating the fidelity of zebrafish orthotopic GBM xenografts in retaining the specific histopathological features of implanting GBM cells.

Single-cell RNA-Seq reveals the transcriptional adaption of GBM cells in zebrafish brain.

Physiological microenvironment has a significant impact on the transcription of tumor cells, which not only affects tumor progression but also therapeutic outcome(Hutchinson and Kirk, 2011). To investigate the transcriptional changes that may arise, zebrafish were implanted with GBM-U-251MG-mCherry cells, which showed a more typical infiltrative growth pattern in the zebrafish brain and facilitate to compare transcriptome changes of infiltrating cells in the zebrafish brain. GBM-U-251MG-mCherry cells were allowed to form widespread, tumor invasion for 4 days. At 4dpi, the core area and tumor invasion area of glioma xenografts were taken out respectively. Finally, scRNA-seq was applied to compare the transcriptome of GBM-U-251MG-mCherry cells isolated from zebrafish orthotopic xenografts with *in vitro* cultured cells (Fig.2A).

Principle component analysis (PCA) showed cultured GBM tumor cells consistently clustered together and apart from the cells isolated from zebrafish brain (Fig.2B). Within the cluster harboring GBM cells from zebrafish brain, core cells (tumor cells in xenograft core) and infiltrating cells (tumor cells infiltrating in parenchyma) were mixed. Unsupervised hierarchical cluster analysis was also used to computationally compare gene expression profiles of the 21 sequenced cells and gave similar results (Fig.2C). Gene Ontology (GO) analysis was performed to characterize and group all differentially expressed genes between these two populations (padj<0.005, up= 346,

down=126) (Table S1). In addition, in zebrafish xenograft derived GBM cells, significant GO enrichment categories relevant to tumor metastasis were obtained, including cell migration and hypoxia response (Fig.2D).

Several genes enriched in zebrafish GBM xenografts were highly relevant to epithelial-to-mesenchymal transition (EMT) and cell migration, including upregulated VIM, TWIST1 and CTDSP2 (interact with SNAI1) and downregulated CDH5 (Fig.2E). Within the GBM xenograft cells, we also noticed upregulation of genes that can impact the cerebral microenvironment (Fig.2E). We suggest the transcriptional identity of zebrafish GBM xenograft cells is characteristic of GBM tumor cell adaption to the *in vivo* physiological environment of the brain. And therefore more likely resemble invading GBM microtumors observed in the proportionally larger brains of model animals and humans.

Characterization of the zebrafish blood-brain-barrier and modeling its interaction with GBM xenografts.

To develop effective GBM drugs, it will be critical to design and evaluate modalities that can circumvent or overcome the BBB associated with GBM cells. To molecularly characterize the BBB in zebrafish larva, we began our investigation by using scRNA-seq to characterize the transcriptomes of endothelial cells (ECs) isolated from the brain and from the body trunk of zebrafish larvae (5dpf) (Fig.3A). Gene expression profile hierarchical cluster analysis highlighted the differential transcriptomes between

cerebral ECs and trunk ECs (Fig.3B). Using Gene Set Enrichment analysis (GSEA), we then compared the transcriptome of zebrafish cerebral ECs to a set of BBB genes previously identified in humans(Qian et al., 2017) (Table S2). GSEA revealed that most of the BBB-related genes were specifically enriched in the zebrafish cerebral ECs compared to trunk ECs (Fig.3C). We also observed some previously identified cerebral endothelial genes that enriched in zebrafish cerebral ECs (foxc1a and foxf2b) along with ctnnb (β-catenin), a factor recently proved to be essential in developing and maintaining of BBB integrity(Wang et al., 2019) (Fig.3D).

Next, to functionally test the BBB in zebrafish larvae, the BBB tracers were injected 1-2 hours before imaging at 5dpf. Within one hour following tracer injection, most cells in tissue outside of the brain displayed blue nuclear staining (DAPI) and green cytoplasmic fluorescence (NaF), suggesting a free diffusion of tracers. In contrary, in the brain of zebrafish larvae, both tracers were strictly retained in the cerebral vessels, indicating the existence of functional BBB in the brain of zebrafish larvae (Fig.3E).

We next sought to characterize the interaction between GBM cells and the BBB in zebrafish brain at 4dpi (Fig.3F). Interestingly, the low molecular weight dextran tracer was still mainly restricted in tumor vessels, indicating that the tumor associated BBB was not functionally destroyed (Fig.3F, blue panel). Next, we used more sensitive assays including high-resolution confocal intravital imaging (Fig.3G) and quantitative diffusion analysis (Fig.3H) to more carefully characterize the BBB function within the GBM xenografts. Surprisingly, the more sensitive imaging and functional analysis

revealed the limited leakage of blue-dextran and DAPI from the cerebral vessels in the xenografts (Fig.3G-I). These results indicate that GBM microtumor/xenografts in zebrafish brain, whether angiogenic or infiltrative, do not simply destroy the zebrafish BBB, but instead initiate slow and steady local damage to BBB organization and function, which are consistent with the previous investigation in rodent brain(Watkins et al., 2014). In summary, we demonstrate that the zebrafish GBM xenograft model provides a detailed visual readout of structural/functional changes to the BBB in the presence of GBM microtumors/xenografts.

Using zebrafish orthotopic GBM xenografts to identify BBB penetrating drugs.

Given the resolution and speed at which interactions between GBM xenografts and the BBB can be modeled in zebrafish larvae, we next explored the zebrafish GBM xenografts in screening the potential drugs that are able to penetrate the BBB and inhibit GBM tumor cells growth *in vivo*. It is necessary to first examine whether small molecular chemicals placed in water can enter brain tissue by simple diffusion. To rule out the possibility, by adding in the water, we tested two florescent BBB tracers: NaF and DAPI. We found that the zebrafish skin tissue outside the brain and the muscle cells in the trunk can be efficiently labeled with green NaF and blue DAPI in the nucleus, indicating the tracers have penetrated most tissue of the zebrafish (Fig.4A, S5). The exception is the parenchymal cells of the brain, they are not labeled at all, indicating that the NaF and DAPI haven't penetrated the brain parenchyma. However, we found

that the cerebral capillaries are highlighted by NaF and the endothelial nucleus are labeled by DAPI, indicating the tracers are delivered into the brain vessels by blood circulation, but unable to cross the boundaries of brain vessels or BBB. These results suggest that adding small molecules directly to the culture water is a simple, reliable way to test BBB-penetrating drug candidates in the zebrafish model system.

To test whether zebrafish GBM xenograft can efficiently identify BBB-penetrating drugs with *in vivo* activity, we tested 6 drugs that were previously evaluated for Glioma treatment *in vitro* and *in vivo* (Arcella et al., 2013; Bastiancich et al., 2018; Kellie et al., 2004; Kikuchi et al., 2008; Ostermann et al., 2004). The testing procedure was standardized prior to experimentation (Fig.4B). Overall, we found, although all drugs except for Dexamethasone (DEX) were able to inhibit growth of U87MG *in vitro* by 50%-100% (Fig.4C). *In vivo*, only Rapamycin and Temozolomide were able to significantly repress the growth of GBM xenografts (Fig. 4D-E). Rapamycin has been demonstrated efficiently in mice(Arcella et al., 2013), and Temozolomide was FDA approved chemotherapy agent for treating high-grade glioma(Ostermann et al., 2004). The failure of DEX to inhibit the growth of U87MG cells *in vitro* or *in vivo*, is consistent with its known function in managing vasogenic edema by reducing the permeability of cerebral vessels (Fig.4D-E). Doxorubicin, Vincrintine and Gemcitabine inhibits U87MG cells *in vitro* by up to ~100%, they had no detectable effect on GBM xenografts *in vivo* (Fig.4D-E). Previous studies indicate the incapability or inefficient of them in crossing the BBB(Bastiancich et al., 2018; Kellie et al., 2004;

Kikuchi et al., 2008). These results indicate the ability of zebrafish GBM xenografts as an *in vivo* model in identifying the BBB penetrating antitumor drugs.

Zebrafish patient-derived orthotopic xenografts (zPDOX) reveals the intra-tumor heterogeneity of GBM cells from individual GBM patient

To expand the zebrafish GBM model, we next sought to generate PDOX from GBM patients. We firstly tried to establish GBM xenografts by directly injecting fresh GBM cell suspensions from two surgically resected patient samples (GBM#109 and GBM#24). Unfortunately, both fail to propagate in the zebrafish brain and dyed away within 3 days. To circumvent this issue, we applied a short-term culture of the primary GBM cells prior to injection. For each sample, we tested three culturing methods, including the glioma organoid derivation procedure, the classical neurosphere enrichment method and the attached culturing procedure with serum. For the first generation, primary GBM cells grew robustly in all three culture systems and enriched with GFAP$^+$ and Nestin$^+$ GBM cells (Fig.5A). Compared to organoid and neurosphere cultured cells, attached culture GBM cells yielded the highest success rate, 58% (attached cells) vs 25% (neurosphere) and 9% (organoid) (Fig.5A right panel). The differentiation of primary GBM cells was evidenced by the low incidence of Nestin$^+$ cell ratio and the presence of very long pseudopodia and synapse-like structures in the 3D Marigel (Fig.5A and S7). Compared with the organoid and neurosphere culture methods, although serum-containing medium didn't result the highest Nestin$^+$ cell ratio,

it enriches the most tumor cells during a short-term *in vitro* culturing (~7-10 days) (Fig.S7), which, in our setting, is important to produce robust xenografts in zebrafish brain.

Using the lentivirus-mCherry labeling, we further tested passage 2 cells of these two GBM patient samples. These two GBM samples were originally characterized by a radiologist and based primarily on the size of the edematous zone using postcontrast MRI(Yamahara et al., 2010) (Fig.5B,C, purple zone). GBM#109 was defined as highly invasive and GBM#24 was defined as less invasive. After labeling with lentivirus-mCherry, GBM cells from each patient were implanted into the zebrafish brain and by 4dpi, robust xenografts were produced in most of the samples (n=15/17 for GBM#109; n=19/23 for GBM#24). Surprisingly, in contrast to the remarkably consistent xenograft phenotype from GBM cell lines, the xenograft phenotypes of patient-derived cells varied, ranging from infiltrative to demarcated (Fig.5B). Considering the small number of primary GBM cells that were initially implanted in each zebrafish brain, we suspect the phenotype variation of patient-derived xenografts may reflect the well characterized intra-tumor heterogeneity of GBM within individual patient tumor. To quantify the observed variability, we scored and calculated the percentage of infiltrative and demarcated phenotypes in each patient's xenografts. We found that even though there was variability, one phenotype predominated: GBM#109 xenografts were 53% infiltrative while GBM#24 xenografts were 26% infiltrative

(Fig.5B, C and Fig.S8). Ultimately, the predominant phenotype matched the GBM phenotype from each respective patient's MRI.

In summary, we have established a stable method for establishing zPDOX mode of GBM. Our zPDOX procedure can efficiently produce multiple xenografts (dozens) from individual patients within 20 days. Critically, the primary histopathological feature of individual GBM sample can be ascertained by scoring and tallying phenotypes from multiple samples. These encouraging results raise the possibility of using zPDOX for co-clinical drug selection and patient specific treatments.

Comparison of short term temozolomide response in zPDOX with long term prognosis of corresponding temozolomide-treated GBM patients.

Temozolomide (TMZ) is an oral alkylating agent used to treat GBM. Although it can cross the BBB, at least 50% of GBM patients do not respond to TMZ(Lee, 2016). Here, we sought to use the zPDOX model to predict TMZ sensitivity for specific GBM patients. Using our established procedure, we transiently cultured GBM tumor cells from five different patients (Table S3) and generated zPDOX for each. The entire test, from tumor dissection to tumor imaging and measurement, was completed within 20 days following surgery (Fig.6A).

For patient 1, GBM xenografts in the zebrafish brain grew relatively slow (produced n=12 samples on 3dpi and divided into 2 groups). Following 3 days of TMZ treatment, the GBM xenografts almost completely disappeared with only residual

tumor mass detectable in some of the zebrafish brains. Thus, we concluded that p#1GBM xenografts were sensitive to TMZ treatment. Consistently, 6 months later after surgery, the patient(p#1) displayed no detectable tumor progression or relapse following combined radiotherapy and TMZ treatment (Fig.6B). For the other four patients, all established zPDOX grew very robustly (n=12 for p#2, n=12 for p#3, n=13 for p#4 and n=15 for p#5). For each zPDOX, following the same TMZ treatment as we described for p#1 derived zPDOX, quantitative results showed significant inhibition ratio of the xenograft size for p#2 and p#5, but not p#3 and p#4. Critically, 6-7months later, according to the MRI result, p#2 and p#5 showed no indication of tumor progression or relapse. However, for p#3 and p#4, whose zPDOX only showed a weak response to TMZ treatment (have some inhibition tendency, but no significant size inhibition ratio), obvious relapse was detected (6-7 months post-surgery).

By consulting postoperative medical records, we listed immunohistochemistry results of each patient in Table S4. Previous studies (Butler et al., 2020; Lalezari et al., 2013) have found high MGMT expression was significantly associated with poor patient survival or treatment response, which resulted in TMZ treatment resistance. Indeed, pathological diagnostic results indicated high level of MGMT expression and high percentage of ki67^{+} tumor cells (#p3 60%, #p4 50%) in the two patients with relapse. Thus, our results altogether indicate that short-term TMZ response in zPDOX is strongly correlated with the incidence of tumor relapse in TMZ-treated GBM patients (6-7 months post-surgery), indicating the ability of zPDOX in predicting the long term

clinical TMZ sensitivity or resistance of the residual GBM micrometastases in patients after surgery.

Although we have not yet gathered sufficient patient numbers to reach statistical significance, we provide compelling evidence from our proof-of-concept experiments that a larger clinical study is warranted. This larger study will help determine whether a short-term TMZ sensitivity assay in our zPDOX model can accurately predict long-term patient response to TMZ. Going forward, this assay will also likely be applicable to rapidly test of the response for other novel drugs or drug combinations.

Discussion

Orthotropic GBM animal models based on mouse and rat are valuable tools that are widely used in studies of cancer biology and drug discovery(Jacobs et al., 2011). However, these rodent-based GBM orthotropic models, whether transplanting either GBM cell lines or patient-derived primary GBM cells, are generally expensive and time consuming and studies are often limited by small experimental numbers and low reproducibility. In the past several years, zebrafish larvae have been introduced as a complimentary animal model to study various human cancers (Fior and Ferreira, 2018; Fior et al., 2017; Yan et al., 2019) and had been successfully used for xeno-implantation of human GBM cells into the zebrafish larva brain (Hamilton et al., 2016; Welker et al., 2017; Welker et al., 2016; Zeng et al., 2017). In our previous

studies, we transplanted human GBM cell lines (U87MG, U-251MG) into the zebrafish brain, and found the small compound, named TNB, could cross the zebrafish BBB and inhibit the progression of GBM cells (Zeng et al., 2017). In addition, Pudelko et al. transplanted both GBM cell lines as well as primary GBM cells into zebrafish blastulas (Pudelko et al., 2018). And they found that GBM cells migrated from zebrafish blastomeres into zebrafish brain after 24 hours post transplantation. Despite the unique advantages of the zebrafish larvae model system, including optic transparency, a naturally immature immune system and the large number of offspring produced for experimentation, the zebrafish based GBM xenograft model is still not widely utilized in the GBM research field. This lack of utilization belies these and other documented experimental strengths. Here, we demonstrate that the zebrafish larva is a versatile model animal for GBM xeno-implantation and provide the most rigorous molecular characterization and histopathological comparison with mammalian models to date. We also demonstrate the existence of a molecularly and functionally intact BBB in zebrafish larva, which allowed the study of interactions between infiltrating tumor cells and the BBB, enabled us to carry out a proof-of-concept screening of BBB-penetrating drugs and predict drug sensitivity for individual GBM patients.

With our zebrafish model, we were able to monitor and document extensive intracranial invasion and tumor vascularization within GBM xenografts. Critically, we show that these characteristics vary depending on the source of implanted GBM cells and reveal the unique cellular responses that exist between and within GBM tumors.

While intracranial invasion and redundant tumor vasculature are not only the most typical pathological features of human GBM, but also key factors that affect the prognosis and radiochemotherapeutic response in GBM patients(Hutchinson and Kirk, 2011; Kamb, 2005). By comparing our outcomes with previously published rodent based GBM xenografts, we show that the zebrafish GBM xenografts can accurately phenocopy the specific histopathological characteristics of individual GBM cell lines. Moreover, for each specific GMB cell line, when dozens of zebrafish xenografts were produced, the phenotype of the implanted xenografts are highly consistent and stable. These data demonstrate that GBM xenografts of diverse origins can consistently and robustly propagate in zebrafish brain and that the zebrafish model system can faithfully reveal the histopathological heterogeneity of implanted GBM cells, indicating it is a reliable animal model for biological and therapeutic studies of intracranial GBM microtumors.

Given the importance of the BBB for efficient delivery of GBM therapeutics, establishing reliable BBB models has been a top priority for GBM drug discovery. Although *in vitro* BBB models(Pardridge, 2005; Qian et al., 2017) have provided greater insight into specific aspects of GBM-associated BBB, they fail to capture the many complexities of the *in vivo* system, especially the dynamic interactions that occur between infiltrating GBM cells and host vascular cells. In the past, many studies indicated that zebrafish was an easy and convenient model for BBB permeability assessment. By using transmission electron microscopy (TEM) (Fleming et al., 2013),

Fleming A et al. found that the structure of zebrafish BBB was gradually formed from 3 dpf and 10 dpf, which was similar to BBB structure of mammalian. In addition, previous studies (Li et al., 2017; Zeng et al., 2017) verified the BBB of zebrafish by using fluorescence tracer with different molecular weight, and found fluorescence tracer was restrained in cerebral capillaries. However, the molecular and functional integrity of BBB in zebrafish larva is unclear, and its possible interaction with implanted GBM tumor cells is not characterized yet. This information, relating to both the pathological behaviors of implanted GBM cells and the brain microenvironment of zebrafish larva, is the fundamental basis for a reliable human GBM orthotopic xenograft model and the possible application in therapeutic tests and drug screens.

Here, by using single-cell RNA-Seq and tracers of BBB function, we rigorously characterized the functional and molecular integrity of the BBB in zebrafish larva. This work, in combination with zebrafish GBM xenografts and fluorescent BBB tracers, allowed us to establish live, *in vivo* imaging of the structural and functional changes that occur to the GBM tumor associated BBB. Interestingly, as shown in previous mouse studies, we observe that the vascular structure in GBM xenografts are constantly altered and, although not completely disrupted, the BBB function was gradually breached. As the BBB is significant barrier to drugs penetrating GBM tumors, a breached BBB could potentially allow drugs access to a developing tumor. Although our model reveals that infiltrating GBM cells can breach the BBB, the magnitude of local BBB breaching from infiltrating GBM cells is likely insufficient to allow drug

penetration in meaningful quantities. This is consistent with reports showing that in brain regions experiencing tumor invasion are typically not enhanced by MRI(van Tellingen et al., 2015), even those with obvious peritumor cerebral edema. Use of our zebrafish should help lead to a more profound structural and molecular understanding of how infiltrating GBM tumor cells dynamically interact with cerebral vasculature and the BBB and aid in the rational design of therapeutic strategies to improve the delivery of antitumor agents.

By optimizing an initial transient culture method, we have established a GBM PDOX model characterized by a high success rate for GBM propagation and rapid turnover time. We also demonstrate that the zPDOX model can accurately replicate and reveal patient specific GBM phenotypes making it a potentially powerful predicative tool for clinical outcomes. However, the number of tested patients is relatively small in this study, the degree to which drug efficacy in zPDOX predicts activity in human patients remains to be determined and a future parallel study including more GBM patient samples is worth a try.

Although zebrafish larvae offer many useful advantages, it still has some inherent limitations compared with mouse-based PDX. For example, human tumor cells and zebrafish have different maintained temperature, and tumor growth could be affected below 37°C. In addition, zebrafish larvae lack the human immune environment. Recent studies have established PDX models in humanized mice, which offers the added advantage over standard PDX models of assaying patient specific tumor response in the

mouse brain, and it could better retain the biological and molecular features of human tumor (Welker et al., 2016; Zeng et al., 2017).

Overall, we have now established an alternative PDOX model using the zebrafish larvae. As the number of GBM cells implanted into a single zebrafish is relatively small, dozens of xenografts can be established from very small piece of patient GBM tissue. This allows for analysis of several samples per patient which increases the chances of detecting internal clonal heterogeneity of the primary GBM which can impact clinical prognosis and treatment plans. Given these advantages of a high success rate, speed and high sample numbers per patient, the zPDOX model will be useful for rapidly evaluating drug response for clinical decisions in precision medicine.

Acknowledgements

Conflict of interest

The authors declare no competing interests.

Ethics Statement

The study protocol was approved by the institutional review board of the Medical Faculty at the West China Hospital, Sichuan University. Written informed consent was obtained from all patients. All zebrafish experiments were conducted in accordance with the guidelines of the Animal Care and Use Committee of Sichuan University (Chengdu, Sichuan, China) and approved by the institutional review board of the Medical Faculty at the West China Hospital, Sichuan University.

Data Availability Statement

The single cell RNAseq data generated in this study is available in GEO under accession number GSE147526, while it remains in private status: elwzgisiptytjap (https://www.ncbi.nlm.nih.gov/geo/query/acc.cgi?acc=GSE147526). Other data that supports the findings of this study are available from the corresponding authors upon request.

Author contributions

C.J.Z., D.C., X.L.A. and Z.P.P.Y. conceived the project. X.L.A., Z.P.P.Y. and C.X.X. established orthotopic Glioblastoma xenografts. X.L.A., C.X.X, J.Z., D.M.Z., X.J.S. and Y.Q.Y. performed confocal images and imaging analysis. X.W., D.C., Y.Y., L.Z. and Z.P.P.Y. collected human tissue and analyzed clinical data. C.J.Z., D.C., X.L.A., Z.P.P.Y., J.J.L. and C.C. wrote the manuscript with input from the remaining authors. X.L.C. and X.Y.P. performed bioinformatic analysis.

Reference

Ai, X., Ye, Z., Yao, Y., Xiao, J., You, C., Xu, J., Huang, X., Zhong, J., Fan, M., Song, X. et al. (2020). Endothelial Autophagy: an Effective Target for Radiation-induced Cerebral Capillary Damage. *Sci Rep* **10**, 614.

Arcella, A., Biagioni, F., Antonietta Oliva, M., Bucci, D., Frati, A., Esposito, V., Cantore, G., Giangaspero, F. and Fornai, F. (2013). Rapamycin inhibits the growth of glioblastoma. *Brain Res* **1495**, 37-51.

Bastiancich, C., Bastiat, G. and Lagarce, F. (2018). Gemcitabine and glioblastoma: challenges and current perspectives. *Drug Discov Today* **23**, 416-423.

Butler, M., Pongor, L., Su, Y. T., Xi, L., Raffeld, M., Quezado, M., Trepel, J., Aldape, K., Pommier, Y. and Wu, J. (2020). MGMT Status as a Clinical Biomarker in Glioblastoma. *Trends Cancer* **6**, 380-391.

da Hora, C. C., Schweiger, M. W., Wurdinger, T. and Tannous, B. A. (2019). Patient-Derived Glioma Models: From Patients to Dish to Animals. *Cells* **8**.

Farin, A., Suzuki, S. O., Weiker, M., Goldman, J. E., Bruce, J. N. and Canoll, P. (2006). Transplanted glioma cells migrate and proliferate on host brain vasculature: a dynamic analysis. *Glia* **53**, 799-808.

Fior, R. and Ferreira, M. G. (2018). Reply to Katsu and Baker: Using zebrafish PDX to screen drug sensitivity of endocrine-dependent cancers. *Proc Natl Acad Sci U S A* **115**, E2910.

Fior, R., Povoa, V., Mendes, R. V., Carvalho, T., Gomes, A., Figueiredo, N. and Ferreira, M. G. (2017). Single-cell functional and chemosensitive profiling of combinatorial colorectal therapy in zebrafish xenografts. *Proc Natl Acad Sci U S A* **114**, E8234-E8243.

Fleming, A., Diekmann, H. and Goldsmith, P. (2013). Functional characterisation of the maturation of the blood-brain barrier in larval zebrafish. *PLoS One* **8**, e77548.

Grobben, B., De Deyn, P. P. and Slegers, H. (2002). Rat C6 glioma as experimental model system for the study of glioblastoma growth and invasion. *Cell Tissue Res* **310**, 257-70.

Hamilton, L., Astell, K. R., Velikova, G. and Sieger, D. (2016). A Zebrafish Live Imaging Model Reveals Differential Responses of Microglia Toward Glioblastoma Cells In Vivo. *Zebrafish* **13**, 523-534.

Hubert, C. G., Rivera, M., Spangler, L. C., Wu, Q., Mack, S. C., Prager, B. C., Couce, M., McLendon, R. E., Sloan, A. E. and Rich, J. N. (2016). A Three-Dimensional Organoid Culture System Derived from Human Glioblastomas Recapitulates the Hypoxic Gradients and Cancer Stem Cell Heterogeneity of Tumors Found In Vivo. *Cancer Research* **76**, 2465-77.

Hutchinson, L. and Kirk, R. (2011). High drug attrition rates--where are we going wrong? *Nat Rev Clin Oncol* **8**, 189-90.

Jacob, F., Salinas, R. D., Zhang, D. Y., Nguyen, P. T. T., Schnoll, J. G., Wong, S. Z. H., Thokala, R., Sheikh, S., Saxena, D., Prokop, S. et al. (2020). A Patient-Derived Glioblastoma Organoid Model and Biobank Recapitulates Inter- and Intra-tumoral Heterogeneity. *Cell* **180**, 188-204 e22.

Jacobs, V. L., Valdes, P. A., Hickey, W. F. and De Leo, J. A. (2011). Current review of in vivo GBM rodent models: emphasis on the CNS-1 tumour model. *ASN Neuro* **3**, e00063.

Kamb, A. (2005). What's wrong with our cancer models? *Nat Rev Drug Discov* **4**, 161-5.

Kellie, S. J., Koopmans, P., Earl, J., Nath, C., Roebuck, D., Uges, D. R. and De Graaf, S. S. (2004). Increasing the dosage of vincristine: a clinical and pharmacokinetic study of continuous-infusion vincristine in children with central nervous system tumors. *Cancer* **100**, 2637-43.

Kikuchi, T., Saito, R., Sugiyama, S., Yamashita, Y., Kumabe, T., Krauze, M., Bankiewicz, K. and Tominaga, T. (2008). Convection-enhanced delivery of polyethylene glycol-coated liposomal doxorubicin: characterization and efficacy in rat intracranial glioma models. *J Neurosurg* **109**, 867-73.

Kitange, G. J., Carlson, B. L., Mladek, A. C., Decker, P. A., Schroeder, M. A., Wu, W., Grogan, P. T., Giannini, C., Ballman, K. V., Buckner, J. C. et al. (2009). Evaluation of MGMT promoter methylation status and correlation with temozolomide response in orthotopic glioblastoma xenograft model. *J Neurooncol* **92**, 23-31.

Lalezari, S., Chou, A. P., Tran, A., Solis, O. E., Khanlou, N., Chen, W., Li, S., Carrillo, J. A., Chowdhury, R., Selfridge, J. et al. (2013). Combined analysis of O6-methylguanine-DNA methyltransferase protein expression and promoter methylation provides optimized prognostication of glioblastoma outcome. *Neuro Oncol* **15**, 370-81.

Lee, S. Y. (2016). Temozolomide resistance in glioblastoma multiforme. *Genes Dis* **3**, 198-210.

Li, Y., Chen, T., Miao, X., Yi, X., Wang, X., Zhao, H., Lee, S. M. and Zheng, Y. (2017). Zebrafish: A promising in vivo model for assessing the delivery of natural products, fluorescence dyes and drugs across the blood-brain barrier. *Pharmacol Res* **125**, 246-257.

Mercatali, L., La Manna, F., Groenewoud, A., Casadei, R., Recine, F., Miserocchi, G., Pieri, F., Liverani, C., Bongiovanni, A., Spadazzi, C. et al. (2016). Development of a Patient-Derived Xenograft (PDX) of Breast Cancer Bone Metastasis in a Zebrafish Model. *Int J Mol Sci* **17**.

Ostermann, S., Csajka, C., Buclin, T., Leyvraz, S., Lejeune, F., Decosterd, L. A. and Stupp, R. (2004). Plasma and cerebrospinal fluid population pharmacokinetics of temozolomide in malignant glioma patients. *Clin Cancer Res* **10**, 3728-36.

Pardridge, W. M. (2005). The blood-brain barrier: bottleneck in brain drug development. *NeuroRx* **2**, 3-14.

Patrizii, M., Bartucci, M., Pine, S. R. and Sabaawy, H. E. (2018). Utility of Glioblastoma Patient-Derived Orthotopic Xenografts in Drug Discovery and Personalized Therapy. *Front Oncol* **8**, 23.

Picelli, S., Bjorklund, A. K., Faridani, O. R., Sagasser, S., Winberg, G. and Sandberg, R. (2013). Smart-seq2 for sensitive full-length transcriptome profiling in single cells. *Nat Methods* **10**, 1096-8.

Pudelko, L., Edwards, S., Balan, M., Nyqvist, D., Al-Saadi, J., Dittmer, J., Almlof, I., Helleday, T. and Brautigam, L. (2018). An orthotopic glioblastoma animal model suitable for high-throughput screenings. *Neuro Oncol* **20**, 1475-1484.

Qian, T., Maguire, S. E., Canfield, S. G., Bao, X., Olson, W. R., Shusta, E. V. and Palecek, S. P. (2017). Directed differentiation of human pluripotent stem cells to blood-brain barrier endothelial cells. *Sci Adv* **3**, e1701679.

Shi, J., Li, Y., Jia, R. and Fan, X. (2020). The fidelity of cancer cells in PDX models: Characteristics, mechanism and clinical significance. *Int J Cancer* **146**, 2078-2088.

van Tellingen, O., Yetkin-Arik, B., de Gooijer, M. C., Wesseling, P., Wurdinger, T. and de Vries, H. E. (2015). Overcoming the blood-brain tumor barrier for effective glioblastoma treatment. *Drug Resist Updat* **19**, 1-12.

Wang, Y., Sabbagh, M. F., Gu, X., Rattner, A., Williams, J. and Nathans, J. (2019). Beta-catenin signaling regulates barrier-specific gene expression in circumventricular organ and ocular vasculatures. *Elife* **8**.

Watkins, S., Robel, S., Kimbrough, I. F., Robert, S. M., Ellis-Davies, G. and Sontheimer, H. (2014). Disruption of astrocyte-vascular coupling and the blood-brain barrier by invading glioma cells. *Nat Commun* **5**, 4196.

Wehmas, L. C., Tanguay, R. L., Punnoose, A. and Greenwood, J. A. (2016). Developing a Novel Embryo-Larval Zebrafish Xenograft Assay to Prioritize Human Glioblastoma Therapeutics. *Zebrafish* **13**, 317-29.

Welker, A. M., Jaros, B. D., An, M. and Beattie, C. E. (2017). Changes in tumor cell heterogeneity after chemotherapy treatment in a xenograft model of glioblastoma. *Neuroscience* **356**, 35-43.

Welker, A. M., Jaros, B. D., Puduvalli, V. K., Imitola, J., Kaur, B. and Beattie, C. E. (2016). Standardized orthotopic xenografts in zebrafish reveal glioma cell-line-specific characteristics and tumor cell heterogeneity. *Dis Model Mech* **9**, 199-210.

White, R., Rose, K. and Zon, L. (2013). Zebrafish cancer: the state of the art and the path forward. *Nat Rev Cancer* **13**, 624-36.

Xu, Z., Kader, M., Sen, R. and Placantonakis, D. G. (2018). Orthotopic Patient-Derived Glioblastoma Xenografts in Mice. *Methods Mol Biol* **1741**, 183-190.

Yamahara, T., Numa, Y., Oishi, T., Kawaguchi, T., Seno, T., Asai, A. and Kawamoto, K. (2010). Morphological and flow cytometric analysis of cell infiltration in glioblastoma: a comparison of autopsy brain and neuroimaging. *Brain Tumor Pathol* **27**, 81-7.

Yan, C., Brunson, D. C., Tang, Q., Do, D., Iftimia, N. A., Moore, J. C., Hayes, M. N., Welker, A. M., Garcia, E. G., Dubash, T. D. et al. (2019). Visualizing Engrafted Human Cancer and Therapy Responses in Immunodeficient Zebrafish. *Cell* **177**, 1903-1914 e14.

Zeng, A., Ye, T., Cao, D., Huang, X., Yang, Y., Chen, X., Xie, Y., Yao, S. and Zhao, C. (2017). Identify a Blood-Brain Barrier Penetrating Drug-TNB using Zebrafish Orthotopic Glioblastoma Xenograft Model. *Sci Rep* **7**, 14372.

Zhai, Y., Li, G., Li, R., Chang, Y., Feng, Y., Wang, D., Wu, F. and Zhang, W. (2020). Single-Cell RNA-Sequencing Shift in the Interaction Pattern Between Glioma Stem Cells and Immune Cells During Tumorigenesis. *Front Immunol* **11**, 581209.

Zhao, C., Gomez, G. A., Zhao, Y., Yang, Y., Cao, D., Lu, J., Yang, H. and Lin, S. (2018). ETV2 mediates endothelial transdifferentiation of glioblastoma. *Signal Transduct Target Ther* **3**, 4.

Zhou, Y., Wu, W., Bi, H., Yang, D. and Zhang, C. (2020). Glioblastoma precision therapy: From the bench to the clinic. *Cancer Lett* **475**, 79-91.
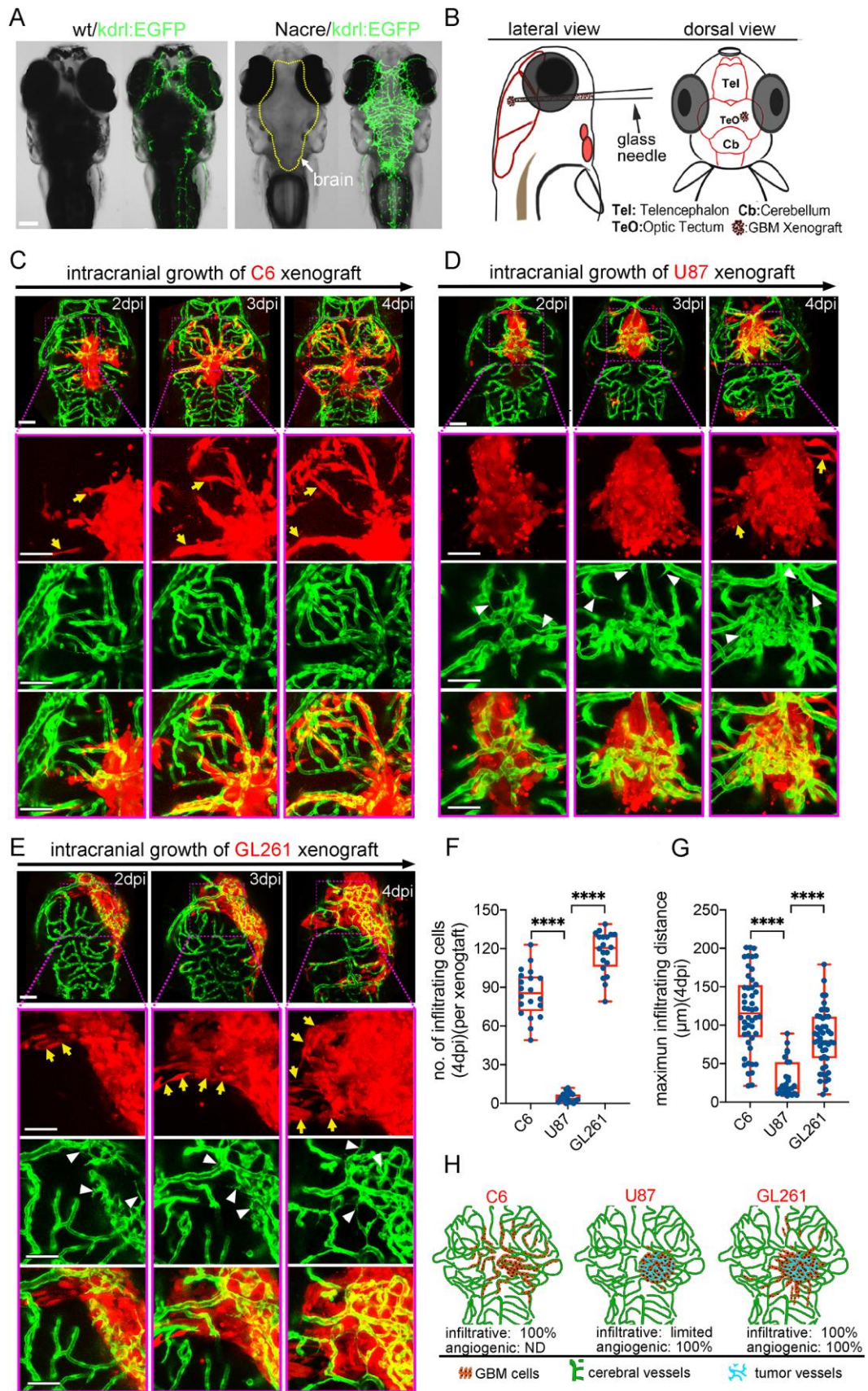
Figures

A wt/kdrl:EGFP | Nacre/kdrl:EGFP

B lateral view | dorsal view

glass needle

Tel: Telencephalon **Cb:**Cerebellum
TeO:Optic Tectum :GBM Xenograft

C intracranial growth of C6 xenograft

2dpi 3dpi 4dpi

D intracranial growth of U87 xenograft

2dpi 3dpi 4dpi

E intracranial growth of GL261 xenograft

2dpi 3dpi 4dpi

F no. of infiltrating cells (4dpi)(per xenogtaft)

C6 U87 GL261

G maximun infiltrating distance (μm)(4dpi)

C6 U87 GL261

H C6 U87 GL261

infiltrative: 100% infiltrative: limited infiltrative: 100%
angiogenic: ND angiogenic: 100% angiogenic: 100%

GBM cells cerebral vessels tumor vessels

Figure 1. Zebrafish orthotopic xenografts reveal the specific *in vivo* histopathological features of implanted GBM tumor cell lines.

(A) Fluorescent stereo microscope of Nacre/kdrl:EGFP zebrafish larvae, showing the clear brain vasculature. (B) Strategy of intracranial implantation of glioma cells into zebrafish larvae. (C) Live tracking of rat C6 xenografts shows extremely infiltrative growing pattern (yellow arrows) associating with rare angiogenesis. (D) Live tracking of human U87MG xenografts shows limited intracranial infiltration, but efficient tumor angiogenesis (white arrowheads). (E) Live tracking of mouse GL261 xenografts shows extremely infiltrative growing pattern (yellow arrows) associating with intensive angiogenesis (white arrows). (F, G) Graphs showing the number of infiltrating cells (per xenograft) and maximum infiltrating distance of each identified invading cells from xenograft edge at 4dpi. n=6-9 brains were counted for each tested GBM xenograft. (H) Graph showing the progressing patterns of individual GBM xenograft in the zebrafish brains. Scale bars, 100μm.
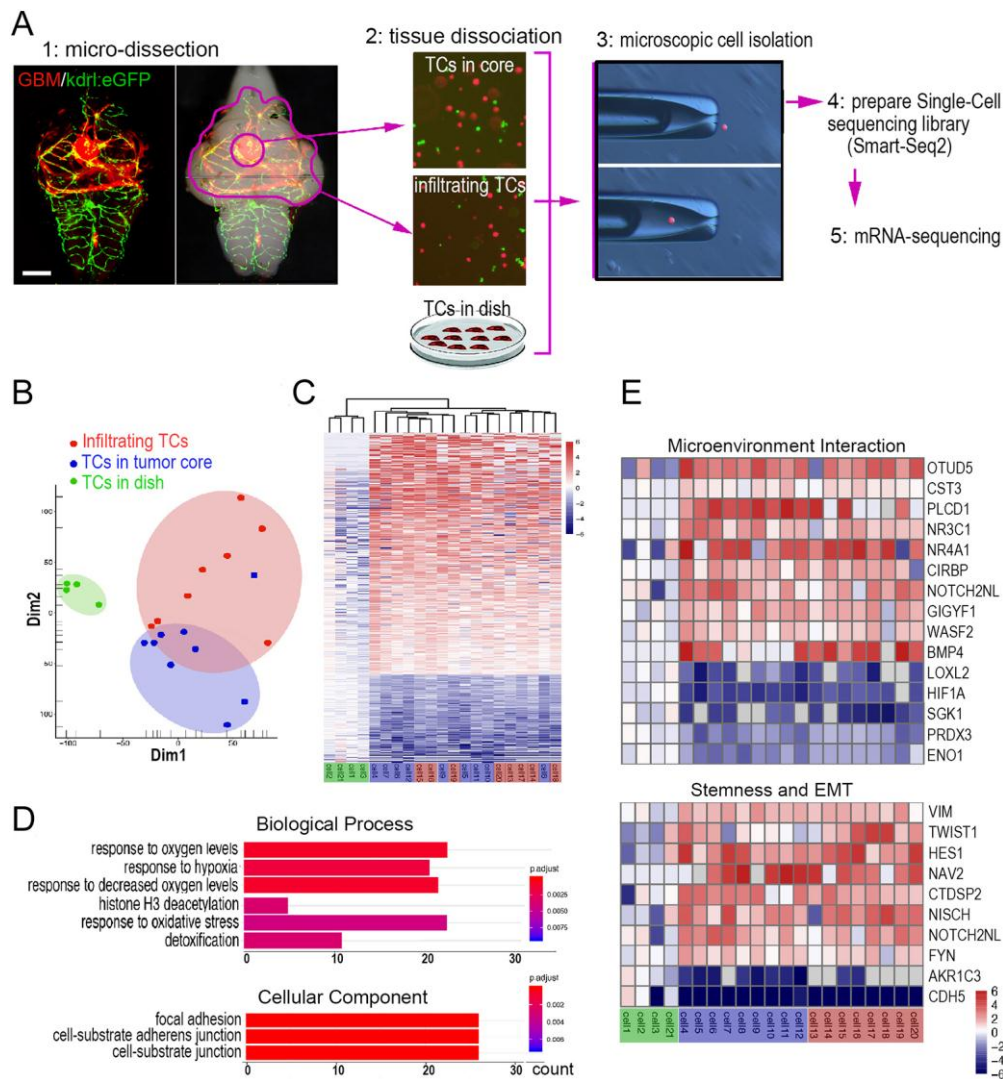
Figure 2. Single-cell RNA-Seq reveals the adaptive changes in transcriptome of GBM xenografts in the zebrafish brain.

(A) Schematic showing the strategy of isolating single GBM-U-251MG-mCherry cells by micromanipulation and preparation of single cell RNA sequencing library basing on Smart-Seq2 protocol. (B) PCA basing on the most variable genes of 21 GBM-U-251MG-mCherry cells, showing distinct patterns of cell clustering. (C) Unsupervised hierarchical cluster analysis basing on all significant differentially expressed genes, showing the similarity of transcriptomes. (D) GO pathway enrichment

analysis basing on the dysregulated differentially expressed genes between the *in vitro* culturing GBM-U-251MG-mCherry cells and those isolated from xenografts. Count: Number of genes relating to the enriched GO. The color of the bars denoting P-value. (E) Heat map basing on the differentially expressed genes of cells from xenografts versus *in vitro* culturing cells.
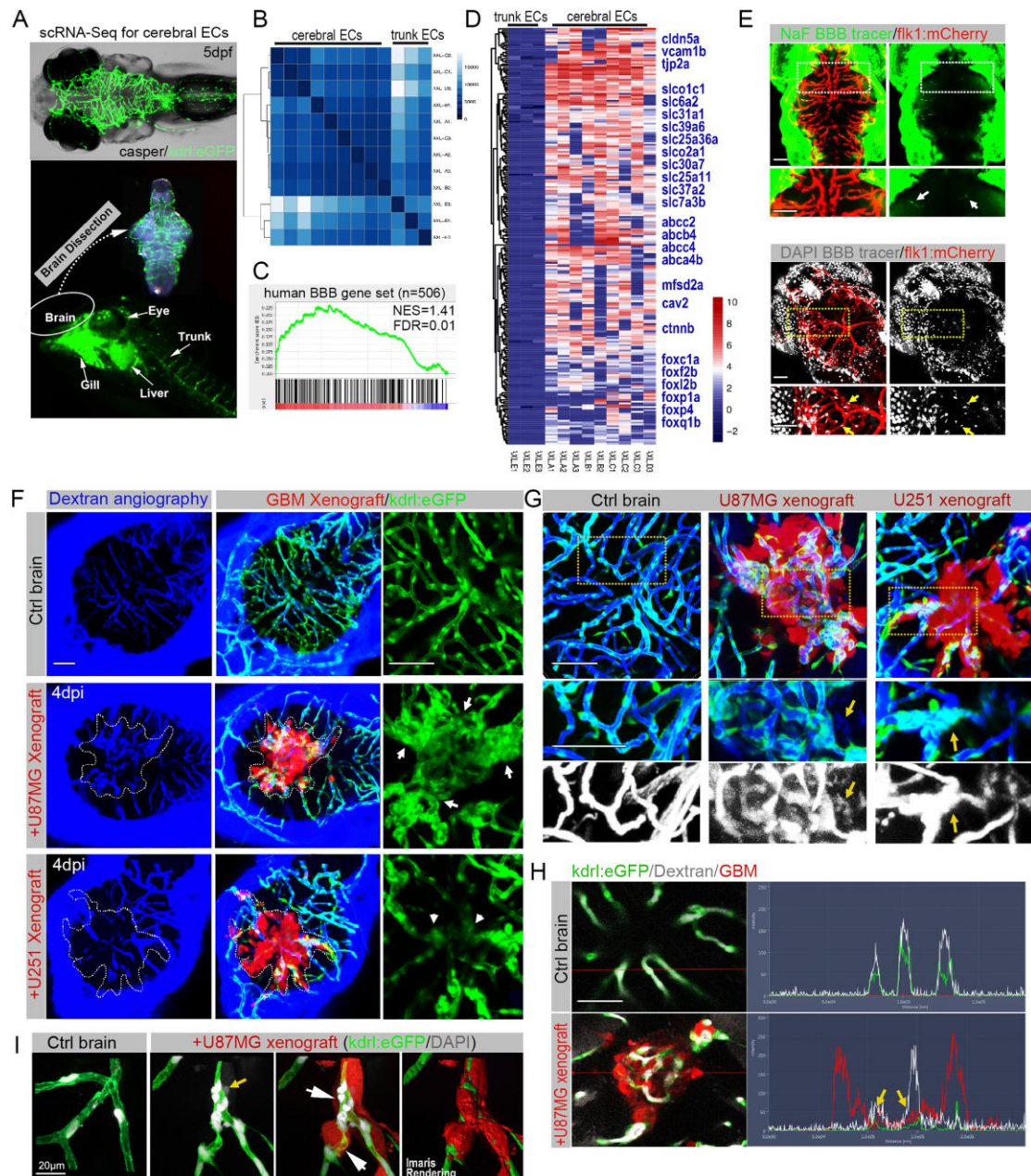
Figure 3. zebrafish GBM xenograft provides a visual readout for the structural and functional changes of tumor-associated BBB.

(A) Schematic showing the strategy of separating cerebral ECs from the trunk ECs of zebrafish larvae. (B) Unsupervised clustering analysis basing on all significant differentially expressed genes of 12 ECs. (C) Gene set enrichment analysis (GSEA) showing the enrichment of BBB genes in zebrafish cerebral endothelial cells. BBB

gene set contains 506 genes including tight junction–related genes, solute carrier transporters, and ATP-binding cassette transporters. (D) Heat map showing the enriched BBB genes in zebrafish cerebral ECs comparing with the trunk ECs. The bar is log2 scaled. (E) living fluorescent microscopy of 5dpf zebrafish heads, showing the incapability of small molecular tracers NaF (MW 376) and DAPI (350 MW) penetrating the brain parenchyma. arrows indicating the BBB tracers that restricted in cerebral capillaries. Areas in dotted area are magnified below. (F) fluorescent microscopy of zebrafish cerebral angiography using Dextran Blue (10,000 MW), showing the intensive angiogenesis (arrows) in U87MG xenograft and vascular degeneration (arrowheads) in U-251MG xenograft. Dotted lines indicating the margin of xenografts. (G) High resolution confocal images of cerebral angiography using Dextran Blue, showing the leakiness (yellow arrows) of tumor vessels in GBM xenografts. Areas in dotted boxes are magnified below. (H) Fluorescent spectrums of blood vessels with Dextran Blue (white signaling) in control brain or GBM xenograft, showing expanding of Dextran Blue signaling (yellow arrows) beyond the vessel boundaries (green signaling) within the xenografts (red signaling). (i) High resolution confocal images of DAPI staining, showing the limited leakage of DAPI (yellow arrow) from blood vessels with infiltrating tumor cells (white arrows). Scale bars, 100μm.
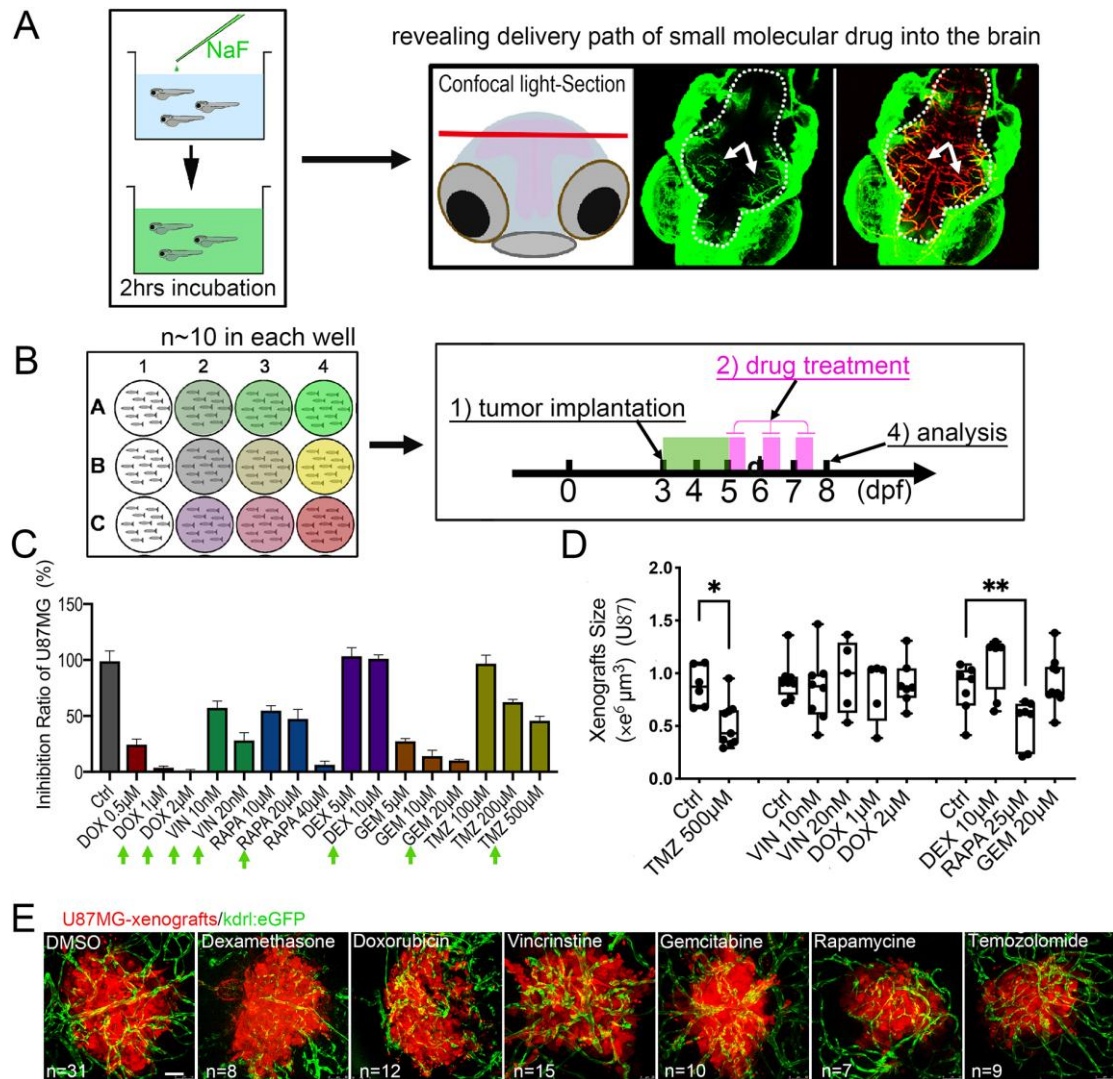
Figure 4. Zebrafish GBM xenografts enable identification of BBB-penetrating drug with *in vivo* activity to the testing GBM.

(A) Schematic showing the small molecular chemical delivering path into the zebrafish brain (5dpf) from culturing water. NaF (376 MW) (10 μM) was added directly into fish water 2 hours before imaging. Within the brain, NaF was restricted in cerebral vessels (arrows), but not freely diffusing in the parenchyma. (B) Schematic showing the strategy of grouping and drug treatment using the zebrafish GBM xenografts (U87MG). (C) Graph shows the growth inhiation ratio of U87MG *in vitro* after 3days treatment by

various drugs at different concentrations. Cell number was tested by MTT assay and the concentrations further tested *in vivo* were marked. (D) graph showing the xenograft size in each group after the drug treatment, showing the significant inhibition by TMZ and RAPA (yellow lines). (E) Representative images of intracranial xenografts (U87MG) after drug treatment, the number of evaluated samples was indicated in the inset. Scale bars, 50μm.
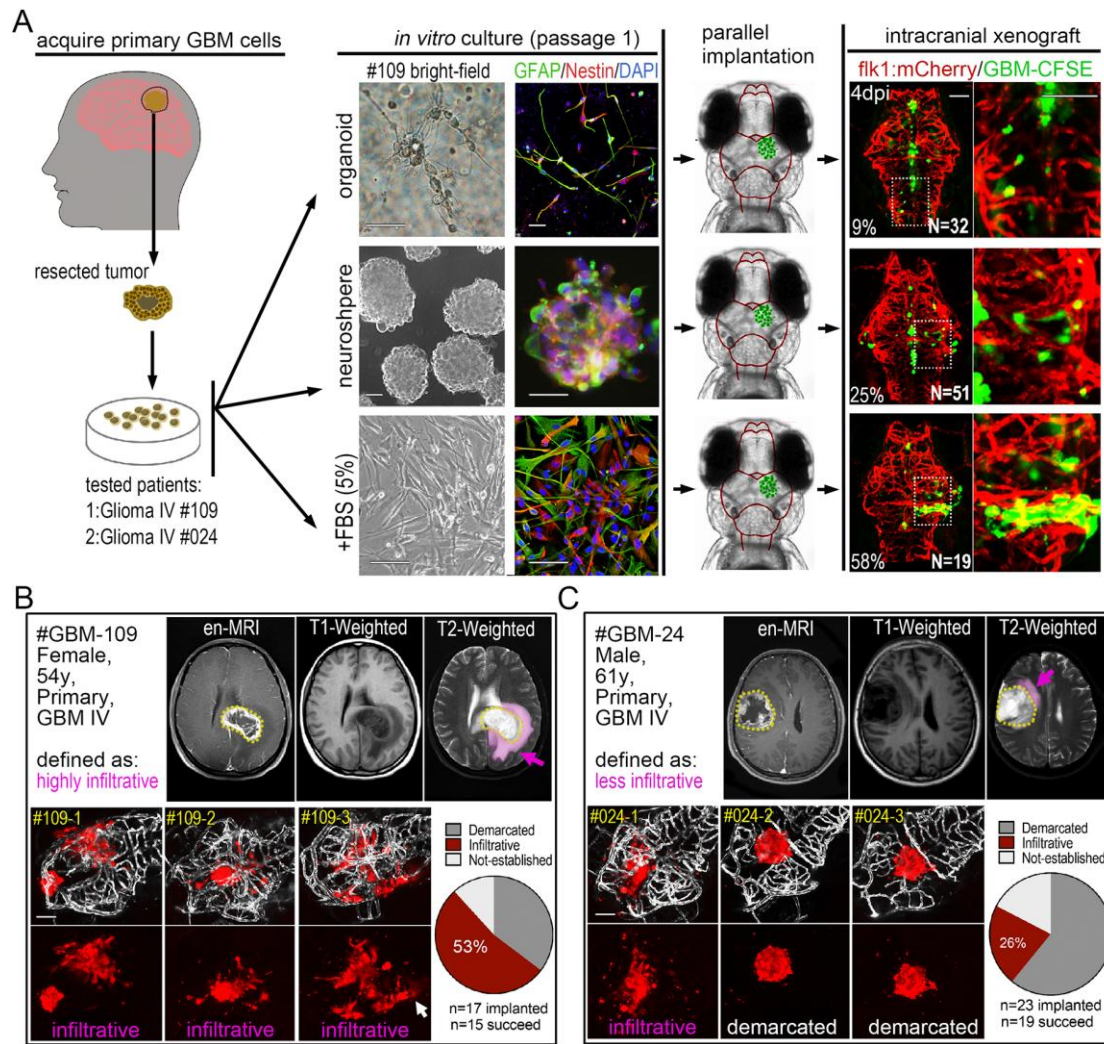
Figure 5. Orthotopic engraftment of patient derived GBM cells into the zebrafish brain.

(A) (left) Schematic showing the acquisition of primary GBM cells from patients. (middle) bright-field and fluorescent microscopy of *in vitro* culturing primary GBM cells (passage 1) from the same patient as 3D organoid, neurosphere and attached single-layer cells. IF staining showing Nestin and GFAP expression differently cultured primary GBM cells. (right) Fluorescent microscopy of 4dpi GBM xenografts from primary GBM cells (passage1). Primary GBM cells were labeled with CFSE before injecting into zebrafish brain. Two patients (GBM#109 Grade IV and GBM#24

Grade IV) were tested. (B, C) Fluorescent microscopy of 4dpi patient derived GBM xenografts from GBM patients, showing the heterogenous phenotypes (infiltrative or demarcated) of primary GBM xenografts. (top) #GBM-109 was defined as highly infiltrative my MRI and #GMB-24 was defined as less infiltrative, purple labeling (purple arrows) in MRI images indicate the edema zone and potential infiltrating areas. (bottom) Brain vasculature is high-lighted by fake gray color (kdrl:eGFP). Xenografts - with more than 5 individual infiltrating cell clusters (white arrows) are defined as infiltrative, otherwise are defined as demarcated. The numbers of xenografts with different phenotypes are counted (pie graph). Scale bars, 100μm.
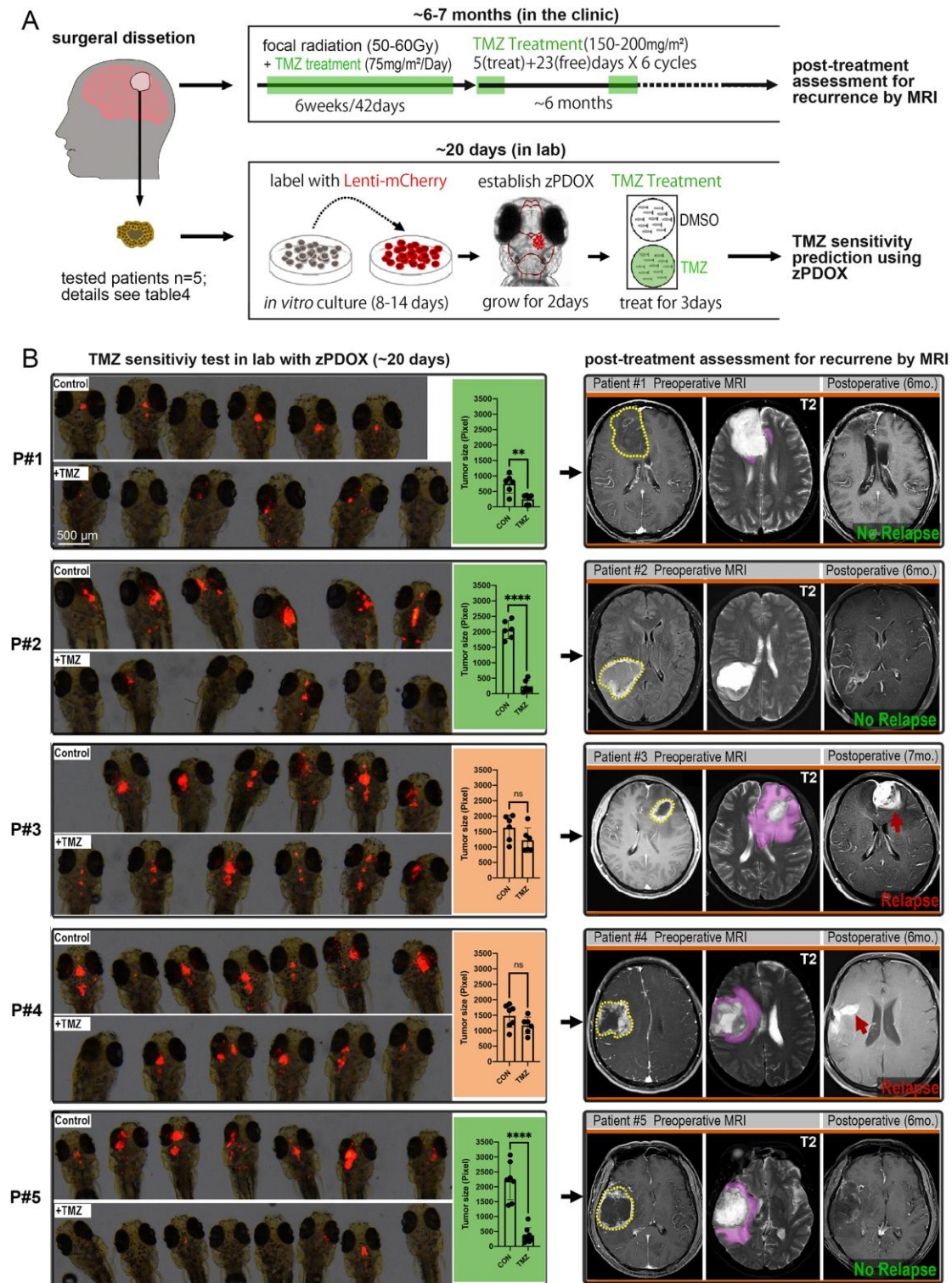
Figure 6. Short-term Temozolomide (TMZ) response in zPDOX predicts the tumor relapse in GBM patients that treated with TMZ.

(A) Schematics shows the procedure of clinical treatment of individual GBM patient and the parallel zPDOX operation in lab. (Right, top) After surgical dissection of the primary GBM tissue, patient was subjected to standard radiotherapy and TMZ chemotherapy. (Right, bottom) Dissected GBM tissue was sent to lab for establishment of zPDOX and TMZ sensitivity test. (B) Comparation of short-term TMZ response in zPDOX in terms of tumor size inhibition ratio and the effect of TMZ to corresponding patient in terms of tumor relapse (6-7month later). Zebrafish recipients with zPDOX were imaged by fluorescent stereoscope and each xenograft was then scanned by confocal and measured by ImageJ. Graphs showing the inhibition ratio of xenograft in terms of tumor size after 3 days' TMZ treatment. *p < 0.05, **p < 0.01, ***p < 0.001, Student's t test. not significant (ns). All five GBM patients were examined before surgery (Preoperative MRI) and about 6~7 months after surgery (Postoperative) by MRI. Gadolinium enhanced tumor (dotted cycles), vasogenic edema (purple zone). Tumor relapse (red arrows). Scale bars, 500μm.
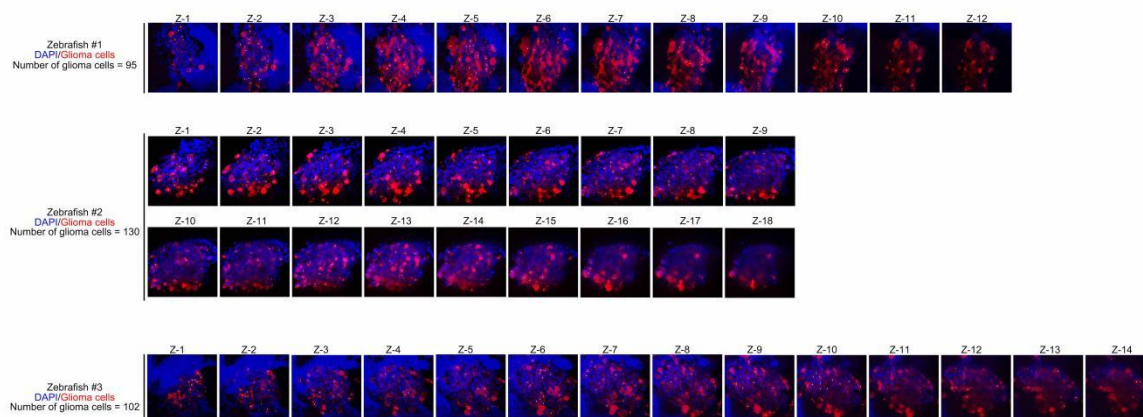
Fig. S1. The whole brain confocal imaging shows three zebrafish GI261-mCherry xenografts. DAPI (blue) and mCherry (red) double positive were marked (white dots) and counted at 2dpi. Scale bar, 50μm.
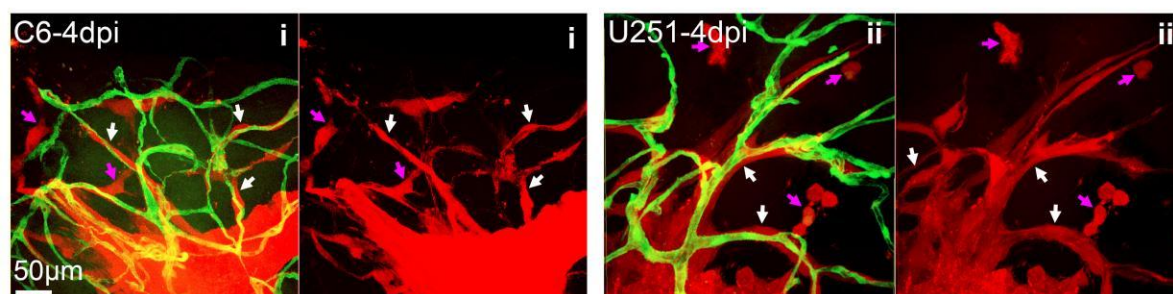

Fig. S2. Image i and ii respectively show the infiltration of rat C6 xenografts (4dpi) and human U251MG xenografts (4dpi) in the zebrafish brain (kdrl:eGFP). White arrows indicate the tumor cells infiltrating along cerebral vessels and magenta arrows indicate the tumor cells invading intraparenchymal. Scale bar, 50μm.

A — 4dpi — GL261

B — 4dpi — kdrlEGFP/GL261

C — 4dpi — kdrlEGFP/GL261

D — GL261 xenografts at 4dpi — #1 #2 #3 #4 #5 #6 #7 #8 #9

E — Demarcated / Infiltrative — 100% infiltrative — n=141

F — 4dpi — U87

G — 4dpi — kdrlEGFP/U87

H — 4dpi — kdrlEGFP/U87

I — U87 xenografts at 4dpi — #1 #2 #3 #4 #5

J — Demarcated / Infiltrative — 100% demarcated — n=277
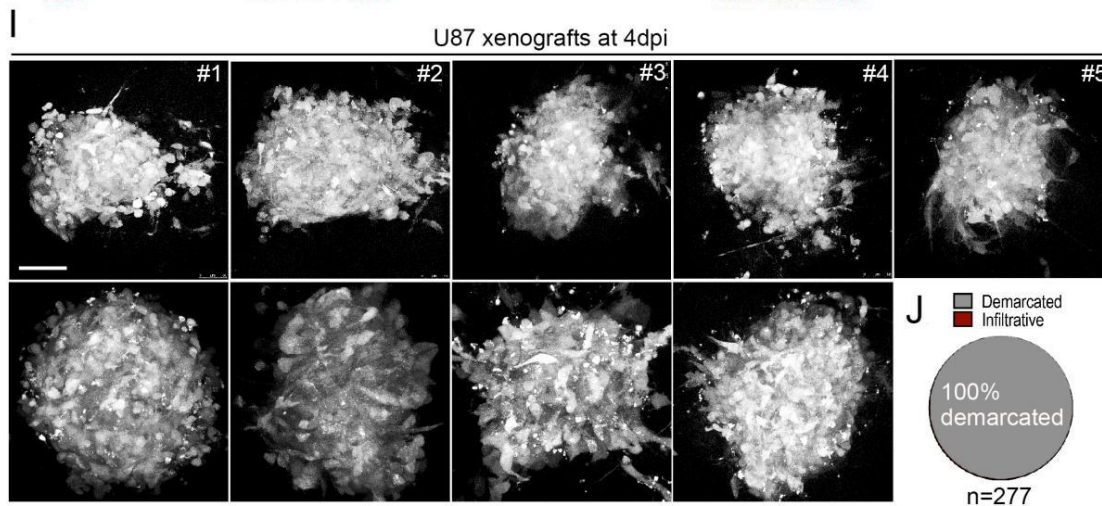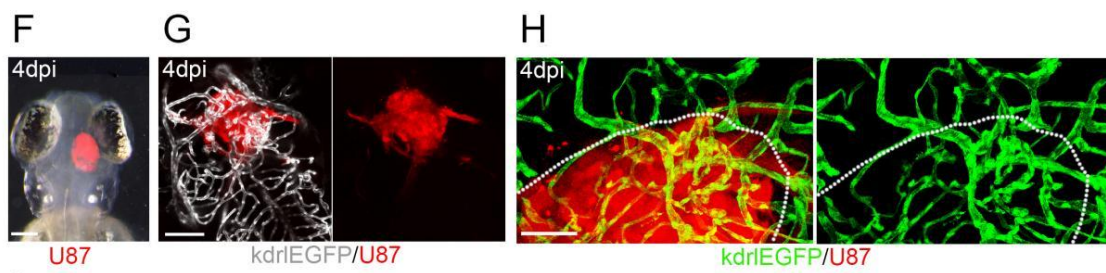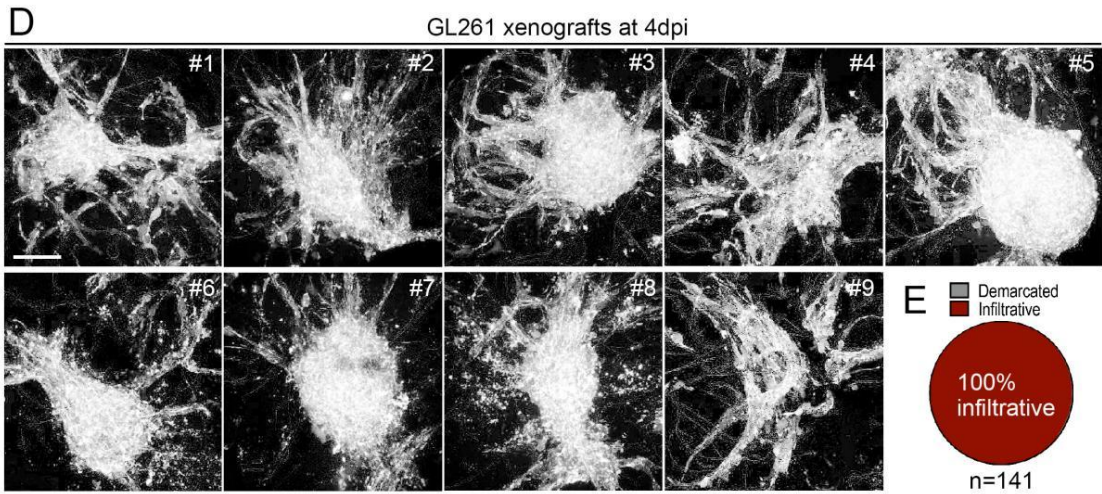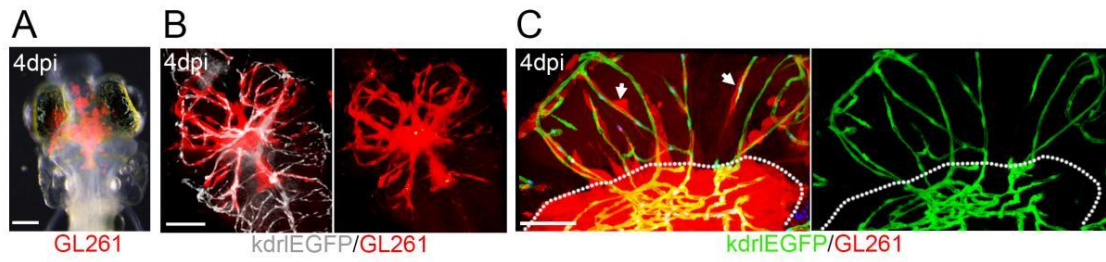
Fig. S3. (A, B) Fluorescent stereo microscope and confocal imaging show the whole brain infiltration of GL261 cells at 4dpi in the zebrafish brain. (C) Confocal imaging shows the extensive infiltrating of GL261 cells (white arrows) along the cerebral capillaries (kdrl:EGFP), dotted line indicating the xenograft edge. (D, E) Confocal imaging of 9 typical GL261 xenografts shows the stable and homogenous infiltrative growing pattern in the zebrafish brain at 4dpi. Totally n=141 GL261 xenografts were evaluated. (F, G) Fluorescent stereo microscope and confocal imaging show the demarcated U87MG xenograft at 4dpi in the zebrafish brain. (H) Confocal imaging shows the tumor angiogenesis within the U87MG xenograft, dotted line indicating the xenograft edge. (I, J) Confocal imaging of 9 typical U87MG xenografts shows the stable and homogenous demarcated growing pattern in the zebrafish brain at 4dpi. Totally n=277 U87MG xenografts were evaluated. Scale bars, 100μm.
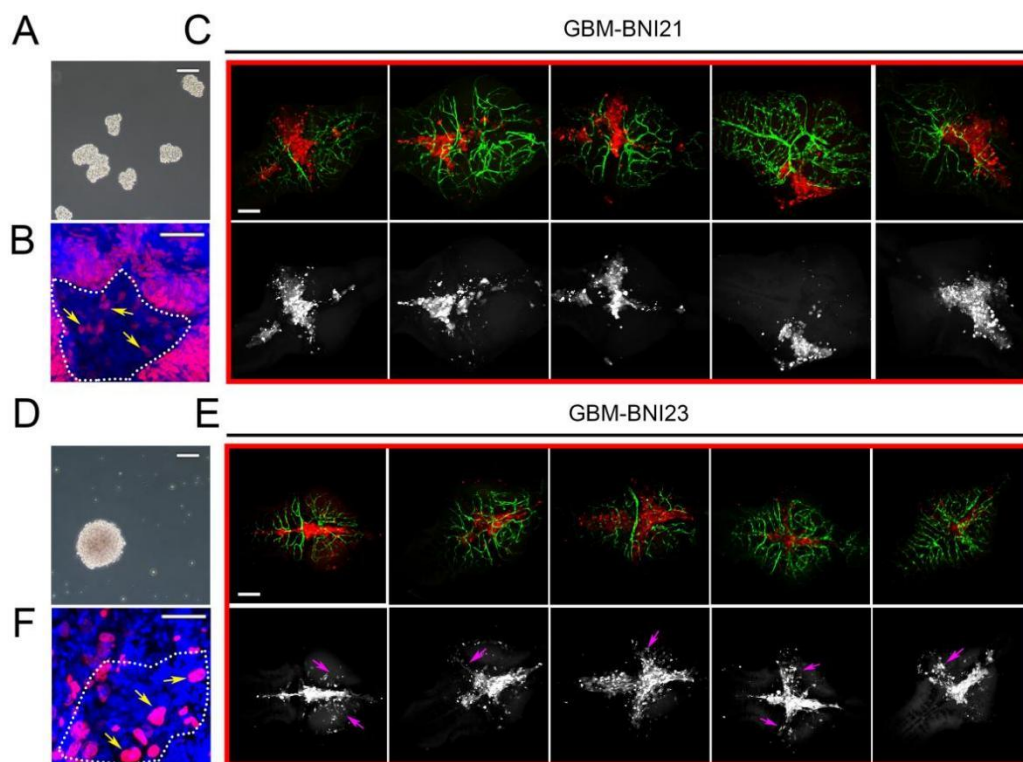
Fig. S4. (A, D) Bright-field of in vitro culturing patient derived GSCs (BNI21, BNI23). (B, F) The tumor confocal imaging shows zebrafish xenografts of BNI21 and BNI23 at 5 dpi. DAPI (blue) and EdU (red) double staining was applied at 5 dpi. EdU positive tumor cells (yellow arrows). (C, E) At 5dpi, BNI23 showed a typical infiltrative growth pattern of GBM in the zebrafish brain. Scale bars, 100µm.
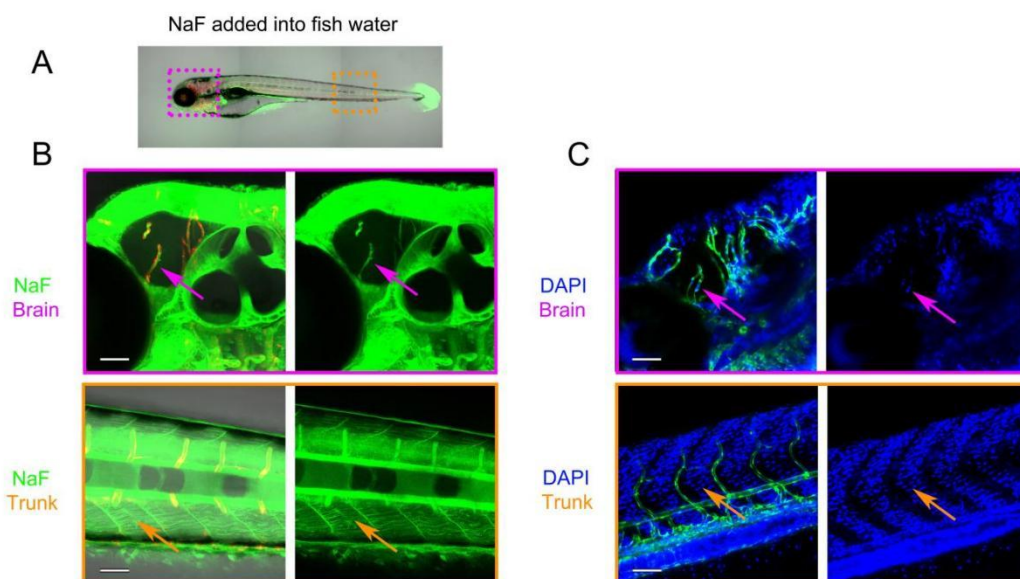
Fig. S5. (A) Schematic showing the BBB tracer NaF penetrating zebrafish tissue (5dpf) from culturing water, areas in the dotted boxes are magnified in B. (B) NaF (376 MW) (10µM) was added directly into fish water 2 hours before imaging. Within the brain, NaF is restricted in cerebral vessels (Magenta arrows), but not freely diffusing in the parenchyma. Within the trunk, NaF is diffused into the muscle fibers (orange arrows). (C) DAPI (2µg/ml) was added directly into fish water 2 hours before imaging. Within the brain, the cerebral endothelial nuclei are labeled by DAPI (Magenta arrows), while the nuclei of parenchymal cells outside of cerebral vessels are not labeled (purple arrow). Within the trunk, the nuclei of muscle fibers are labeled by DAPI (orange arrow). Scale bars, 100µm.
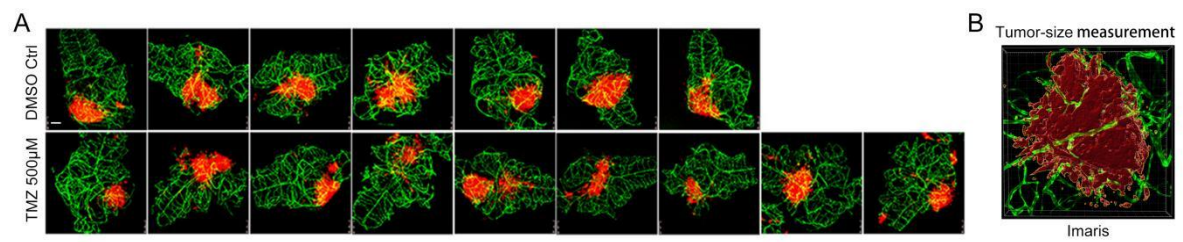
Fig. S6. (A) images show the U87MG xenografts (red) in the dissected zebrafish brains (kdrl:eGFP) after treated by temozolomide (TMZ, 500µM) for 3 days. (B) Representative image shows the measurement of xenograft by Imaris. Scale bars, 100µm.
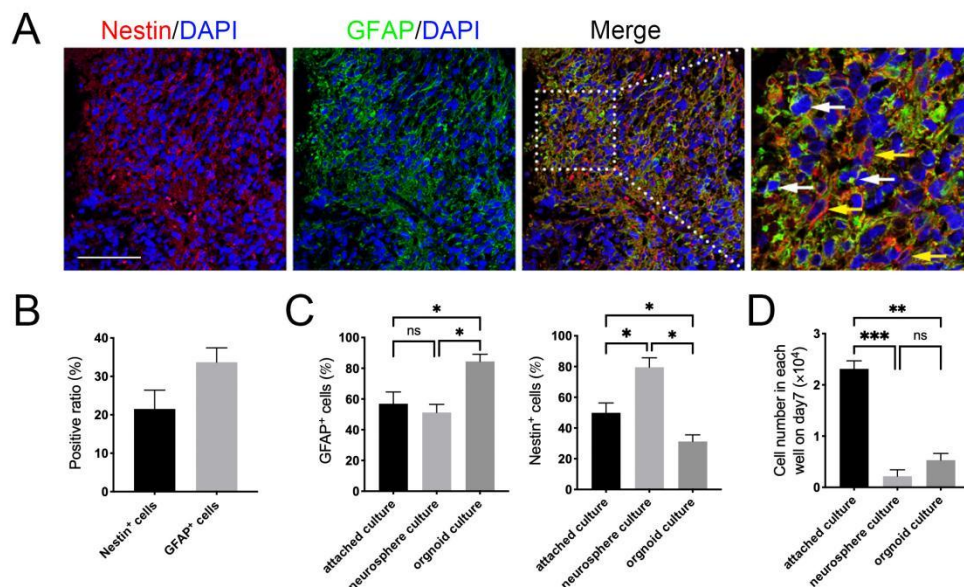
Fig. S7. (A) Patient GBM tissue stained for Nestin[+] (red, yellow arrows) and GFAP[+] (green, white arrows). (B) Quantification of Nestin[+] and GFAP+ ratio. (C) Graph shows the percentage of Nestin[+] and GFAP^{+} cells (Passage 1) in the different transient culture systems (Attached culture, Neuroshpere culture and Organoid culture), Nestin[+] and GFAP^{+} cells were determined by IF staining. (D) Graph shows the cell numbers that can be enriched in passage1 on day7 from different transient culture systems. GBM#109 was tested in this experiment. Scale bars, 100μm.
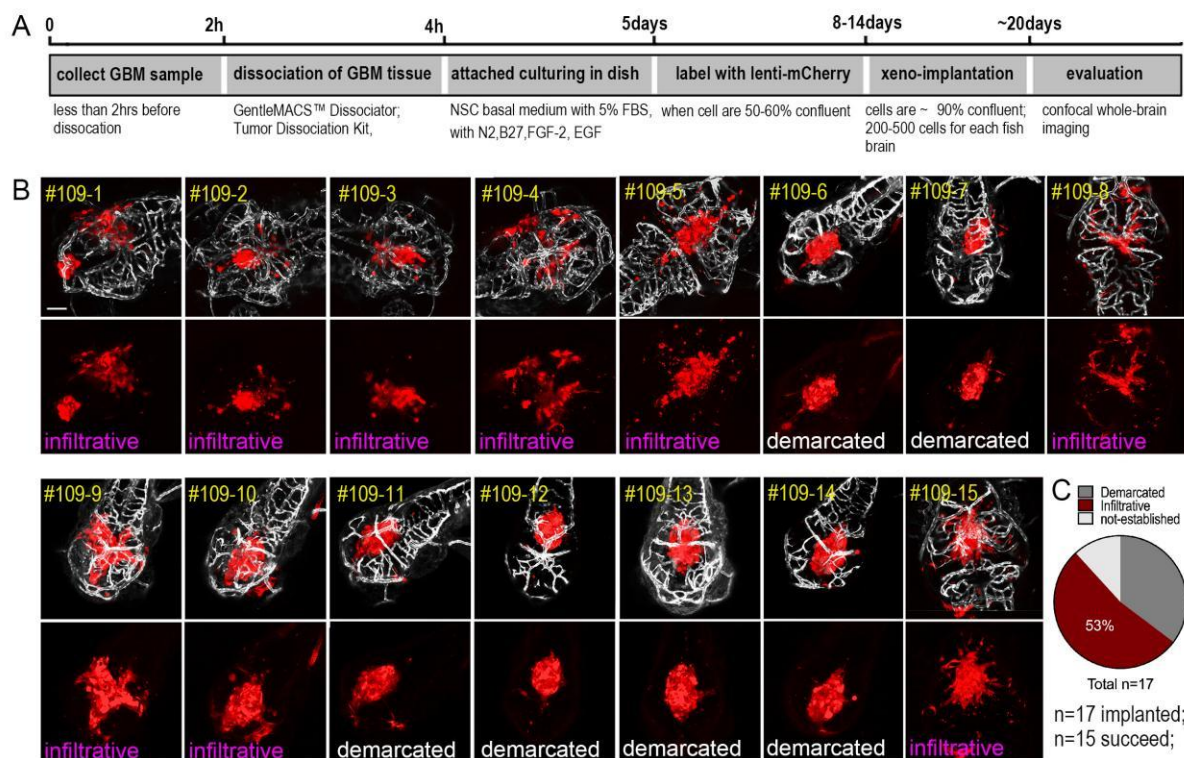
Fig. S8. (A) Timeline shows the procedure of transient *in vitro* culture and implantation of patient derived GBM cells. The culturing time for passage1 (P1) GBM cells varied from 5days to 2weeks, depending on individual patients. (B) Images show the phenotypes of individual patient derived xenografts (n=15, GBM#109, 4dpi) in zebrafish brain (kdrl:eGFP, gray channel), indicating the intra-heterogeneity of primary GBM cells (P1). (C) Diagram shows the percentage of infiltrative and demarcated xenografts in the zebrafish brain, xenograft has more than 5 detached invading cell clusters from the tumor core was defined as infiltrative.

Table S1.

Click here to download Table S1

Table S2. The 506 genes of BBB gene set were enriched in zebrafish cerebral endothelial cells

Click here to download Table S2

Table S3. Summary of the Clinical Data of GBM Patients and Experimental Results Derived from Primarily Cultured GBM Cells

Click here to download Table S3

Table S4. Postoperative Pathological Diagnostic Results of Patients

Click here to download Table S4